Optimizing a Mesenchymal Stromal Cell Product for Treating Bronchopulmonary Dysplasia

By

Celine Fawagreh

Thesis submitted to the University of Ottawa in partial Fulfillment of the requirements for the MSc degree in Cellular and Molecular Medicine

Department of Cellular and Molecular Medicine Faculty of Medicine

University of Ottawa

Abstract

Bronchopulmonary dysplasia (BPD) is the most common and severe chronic lung disease affecting premature infants following exposure to hyperoxia and inflammation, with no cure. BPD leads to arrested alveolar growth, pulmonary hypertension (PH) and lifelong breathing difficulties. Mesenchymal stromal cells (MSCs) are multi-potent cells with anti-inflammatory, immunomodulatory and regenerative properties. We previously showed that umbilical cord (UC)-derived MSCs isolated from different donors provide varying lung-protective effects in experimental BPD. Induced pluripotent stem cells (iPSCs) from a single donor have been proposed to provide a large and homogenous pool of iPSC-derived MSCs (iMSCs). Here, we demonstrate that iMSCs improve indicators of PH in a rat neonatal lung injury model. In comparison, we found that only two out of six UC-MSC donors provided therapeutic benefits. Overall, our work demonstrates that iMSCs from a single donor are possible candidates for treating BPD without inter-donor variability, increasing their potential for successful clinical translation.

Abbreviations

BPD	Bronchopulmonary dysplasia
BW	Body weight
CdM	Conditioned media
CMF	Cell Manufacturing Facility
cDNA	Complementary Deoxyribonucleic acid
DNA	Deoxyribonucleic acid
ESC	Embryonic stem cell
EV	Extracellular vesicle
GA	Gestational age
GvHD	Graft versus Host Disease
H&E	Hematoxylin and eosin
IDO	Indoleamine 2,3-dioxygenase
IFN	Interferon gamma
IL	Interleukin
iMSC	Induced pluripotent stem cell-derived mesenchymal stromal/stem cell
iPSC	Induced pluripotent stem cell
ISCT	International Society for Cell and Gene Therapy
i.t.	Intratracheal
LPS	Lipopolysaccharide
MLI	Mean linear intercept
mRNA	Messenger ribonucleic acid
MSC	Mesenchymal stromal/stem cell
MSC-EV	MSC-derived extracellular vesicle

NO	Nitric oxide
NTA	Nanoparticle Tracking Analysis
OHRI	Ottawa Hospital Research Institute
PAAT	Pulmonary arterial acceleration time
PAET	Pulmonary arterial ejection time
PBS	1X Phosphate buffered saline
PCR	Polymerase chain reaction
P	Postnatal day
PH	Pulmonary hypertension
PN	Passage number
Ppl	Pressure plethysmography
PV-loop	Pressure-volume loop
qPCR	Quantitative real time-polymerase chain reaction
RA	Room air
RDS	Respiratory distress syndrome
RNA	Ribonucleic acid
RT-qPCR	Reverse transcription quantitative real-time polymerase chain reaction
RVH	Right ventricular hypertrophy
scRNA-seq	Single-cell RNA sequencing
SD	Sprague Dawley
STD	Standard deviation
TNF	Tumor necrosis factor alpha
UC	Umbilical cord
VEGF	Vascular endothelial growth factor
Vpl	Volume plethysmography

Table of Contents

List of Figures

List of Tables

Acknowledgments

First and foremost, I would like to thank my supervisor, Dr. Bernard Thébaud, and my co-supervisor, Dr. Dylan Burger, for giving me the opportunity to pursue an MSc in their lab and for providing invaluable guidance and support throughout the whole process. I would also like to express my appreciation to all the wonderful members of the Thébaud lab: Dr. Arul Vadivel, Adithya Achuthan, Dr. Chanèle Cyr-Depauw, Dr. Ewa Henckel, Dr. Liqun Xu, Mahnaz Nazari, Mairead Green, Rhea Mital, Sahar Salari, Shumei Zhong, Dr. Wojciech Durlak for all their help throughout these years. I would also like to extend special acknowledgments to Shumei Zhong, Dr. Arul Vadivel and Dr. Chanèle Cyr-Depauw for their guidance and training on this project.

I would like to express my appreciation to Dr. Chanèle Cyr-Depauw, Dr. Bernard Thébaud and Dr. Dylan Burger for taking the time to edit this dissertation. I would also like to acknowledge Dr. Chanèle Cyr-Depauw, Shumei Zhong and Dr. Arul Vadivel, Dr. Marius A. Möbius and Dr. Saad Khan for their excellent advice and for motivating me throughout. I also want to thank the Cell Manufacturing Facility at OHRI for their collaboration.

I wish to acknowledge my thesis advisory committee members, Dr. William Stanford, and Dr. Jessie Lavoie for providing direction and feedback on this project. I also wish to thank Dr. Jessie Lavoie and Dr. Pierre Mattar for agreeing to evaluate my thesis and defense.

Finally, and most importantly, I would like to thank my parents for believing in me and for always supporting me.

1. Introduction

1.1 Bronchopulmonary dysplasia

1.1.1 Pathophysiology

Bronchopulmonary dysplasia (BPD) is the most common and severe complication in extremely preterm infants (born before 28 weeks of gestational age [GA]) (1–3). BPD is a chronic and multifactorial lung condition characterized by an arrest in alveolar and microvascular growth **(Figure 1 and 2)** (4). In 1967, Northway, Rosen and Porter described "old" BPD as a syndrome which develops in mildly preterm infants (34 weeks of GA) with respiratory distress syndrome (RDS), a lethal condition at the time resulting from surfactant deficiency (5). Treatment interventions for RDS included mechanical ventilation and 80%-100% supplemental oxygen (hyperoxia). While these interventions were an attempt to keep the infants alive, they exposed neonates to prolonged excessive oxygen levels, triggering a pulmonary inflammatory response and lung injury. The authors described BPD as a result of a slow, prolonged recovery of these interventions. Over the past 50 years, advances in perinatal care helped treat RDS and allowed extremely preterm infants to survive using surfactant, corticosteroids and respiratory support devices (6). However, the incidence of BPD increased between 1993 and 2012 in extremely preterm infants (23-28 weeks of GA) as their lungs are very early in their developmental process. This is known as the "new" BPD. Today, around 45% of extremely preterm infants develop BPD worldwide **(Figure 3)** (2,3).

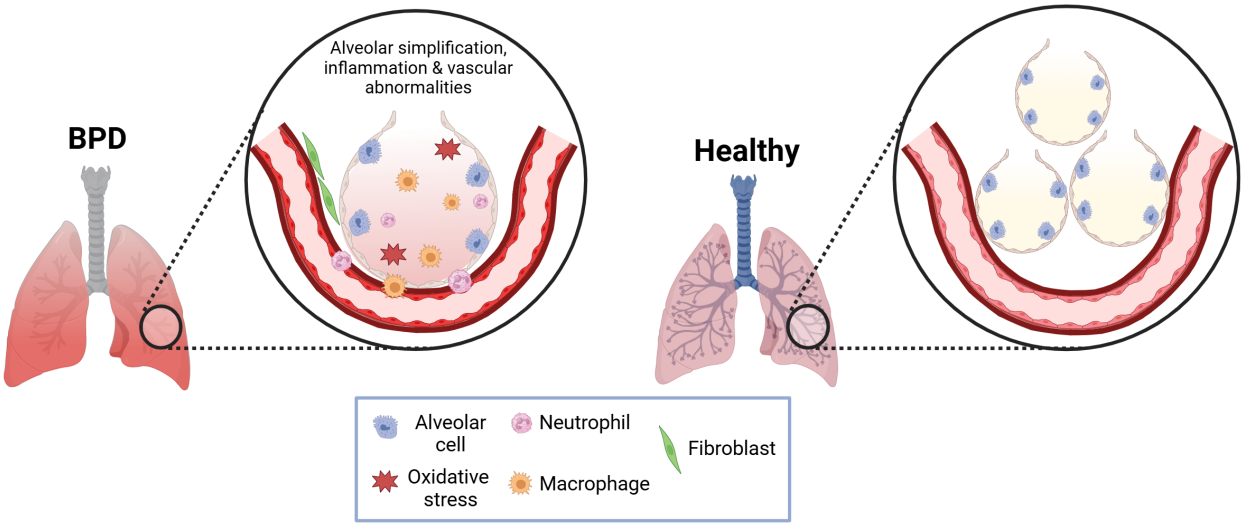

Figure 1. Schematic overview of pathophysiology of bronchopulmonary dysplasia (BPD) compared to a healthy lung. BPD is a multi-factorial disease characterized by an arrest in alveolar growth. Pathological processes lead to oxidative stress and inflammation which affects immunity, vascularization, repair and regeneration. Figure made with Biorender.

In the clinic, BPD is defined by the requirement of respiratory support at 36 weeks post-menstrual age (GA + chronological age). Prenatal risk factors include heritability, tobacco exposure, intrauterine growth restriction, and maternal complications such as chorioamnionitis (intrauterine inflammation) and preeclampsia (abnormal placentation) (7–10). Postnatal risk factors include life-saving interventions such as mechanical ventilation, and oxygen exposure which trigger a pulmonary inflammatory response (11). Under hyperoxic conditions mimicking BPD, it was shown that lung resident macrophages polarize from anti-inflammatory type 2 (M2) macrophages to proinflammatory type 1 (M1) macrophages (12). M1 macrophages secrete lactate, nitric oxide and reactive oxygen species which are cytotoxic (13). However, the exact mechanism of how such pro-inflammatory effects lead to impaired lung development remains unknown.

Factors such as oxygen exposure and mechanical ventilation may lead to the onset of chronic complications such as asthma, emphysema, reduced exercise capacity and pulmonary

hypertension (PH) (14–16). PH is a common consequence of severe BPD (29-58%) which arises from dysregulated lung vascular growth (17). BPD is also characterized by a rampant immune response. Currently, there are still no effective clinically approved treatments for BPD.

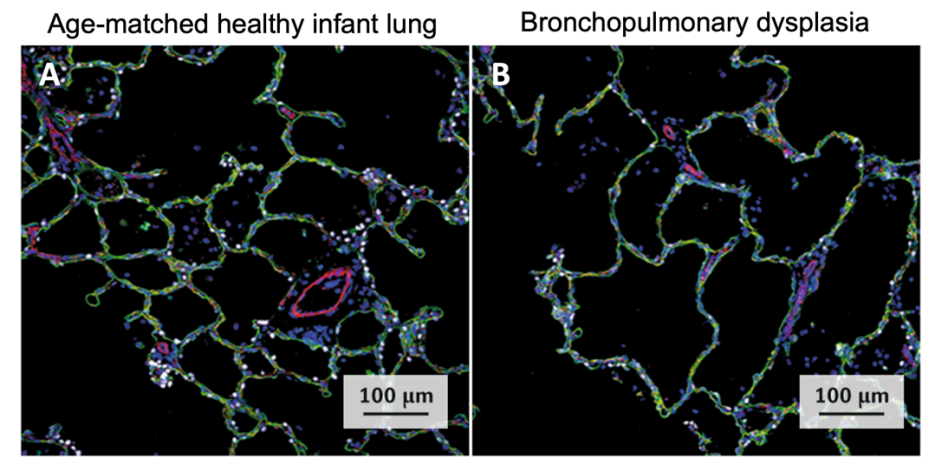

Figure 2. Confocal microscopy images of lung sections from an infant with BPD compared to a healthy infant at ~3 years of age. (A) Lung section of a healthy infant. **(B)** Lung section of an infant with BPD. Alveolar type 1 (AT1) cells are stained with anti- AGER antibodies (green). Endothelial cells in pulmonary capillaries are stained with an anti- PECAM1 antibody (red). AT2 cells are stained with an anti- NKX2.1 antibody (white). Modified from Ref 1.

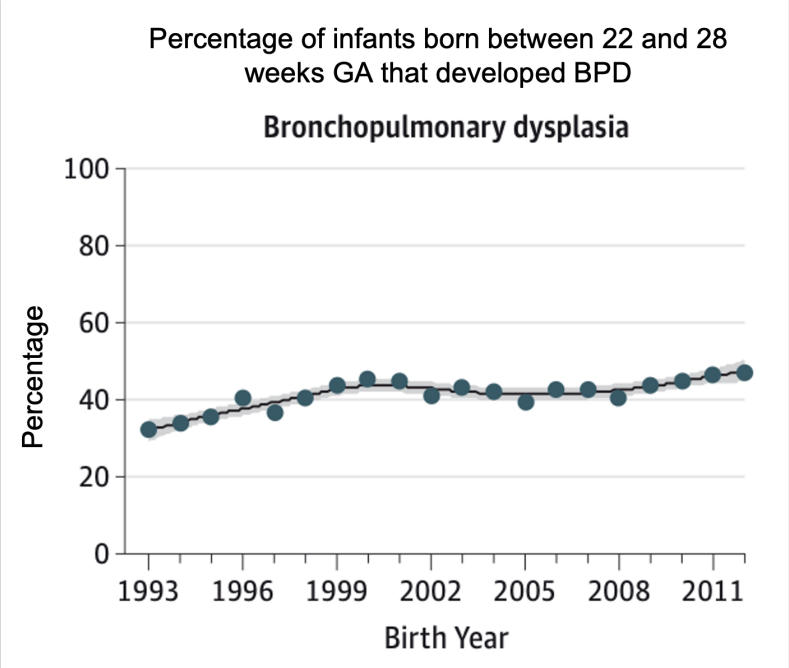

Figure 3. Percentage of infants born between 22 and 28 weeks GA that developed BPD. Dots show the percentage of infants born each year diagnosed with BPD, and the curve shows the trend. Total number of infants (mean [range] per year): 25,000 (1,250 [746-1,534]). Study sites were distributed throughout the United States. Modified from Ref 2.

1.1.2 Current treatments for BPD

Although effective treatments for BPD are lacking, there are several interventions used to minimize lung injury in premature infants. Caffeine is used as a respiratory stimulant which reduces ventilation time and consequently lowers lung injury while also being associated with improved cognitive and motor outcomes (18). However, caffeine has no effects on rates of death, severe hearing loss, or bilateral blindness, which are common complications of prematurity. Surfactant is used to help with gas exchange and reducing ventilation time, however it does not drastically change the outcomes for BPD (19–21). In addition, vitamin A is used to promote lung growth however it only yields a small reduction in death or BPD (22). Furthermore, glucocorticoids such as dexamethasone and hydrocortisone are used as powerful anti-

inflammatory drugs. However, evidence suggests that they cause neurodevelopmental impairment, leading to recommendations against their use (23).

1.1.3 Stages of healthy lung development versus disrupted lung development in BPD

Human lung development consists of 5 different stages: 1) embryonic, 2) pseudoglandular, 3) canalicular, 4) saccular, and 5) alveolar stages **(Figure 4)**. Preterm infants are born in the late canalicular (16 to 26 weeks' GA) and saccular stages (26 to 36 weeks' GA) of lung development (24). At those stages, the primary septa are not effective in forming air-blood barriers to enable normal breathing. The lack of alveoli and limited pulmonary capillary network growth in preterm infants raises the risk of developing disabilities such as RDS, apnea, PH and BPD (25). In fact, premature birth, defined as birth before 37 weeks of gestation, is the leading cause of death in children under the age of five, causing approximately one million deaths worldwide every year (26,27).

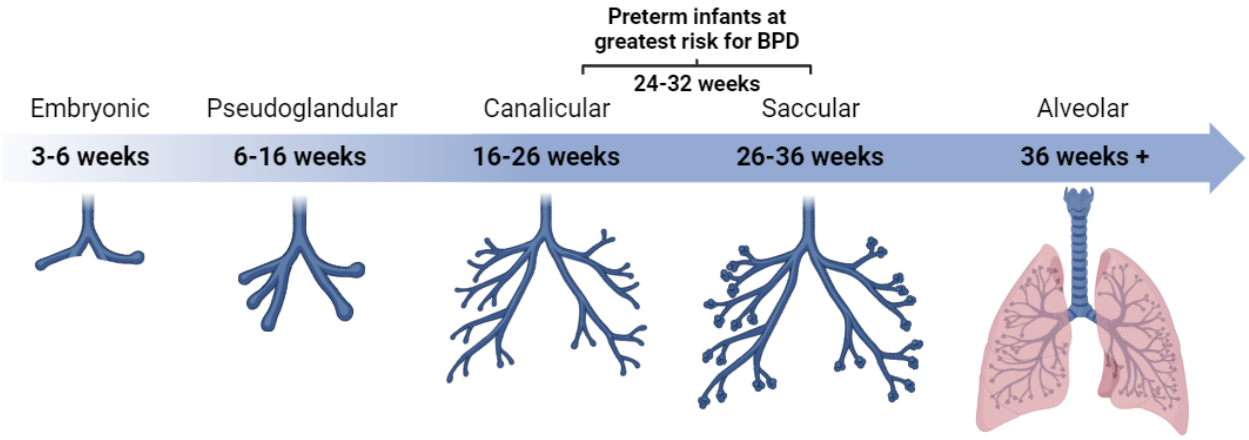

Figure 4. Stages of human lung development. Changes in airway morphology with advancing gestational age are shown. Figure made with Biorender.

1.1.4 Modeling BPD: The advantages of the neonatal hyperoxia-induced rat model

The lack of effective treatments and long-term effects of BPD demonstrate the necessity of *in vivo* research to study the disease. Rats offer several advantages to large animal models and smaller mice models. They are born at term in the saccular stage of lung development, which is similar to the lung developmental stage of preterm infants **(Figure 5)** (28). In addition, rats have a short gestational period, an average of 11 pups per litter and an average weight of 5 grams at birth versus 1 gram for mice. A larger average birth weight would allow for easier surgical manipulations such as intra-tracheal (I.T.) and intra-venous (I.V.) injections. Furthermore, rats have a short lifespan of 24 to 36 months which allows for long-term studies. In fact, long-term studies have shown that exposure to hyperoxia creates long-lasting effects on lung structure and pulmonary vascular function characterized by alveolar simplification and right ventricular hypertrophy (RVH) at 60 days of age (29). In conclusion, neonatal rats contain an element of structural lung immaturity while having a relatively larger size than mice which allows for easier surgical manipulations, more tissue collection at harvest and testing of therapeutic interventions, such as cell therapies, making them appropriate models for BPD.

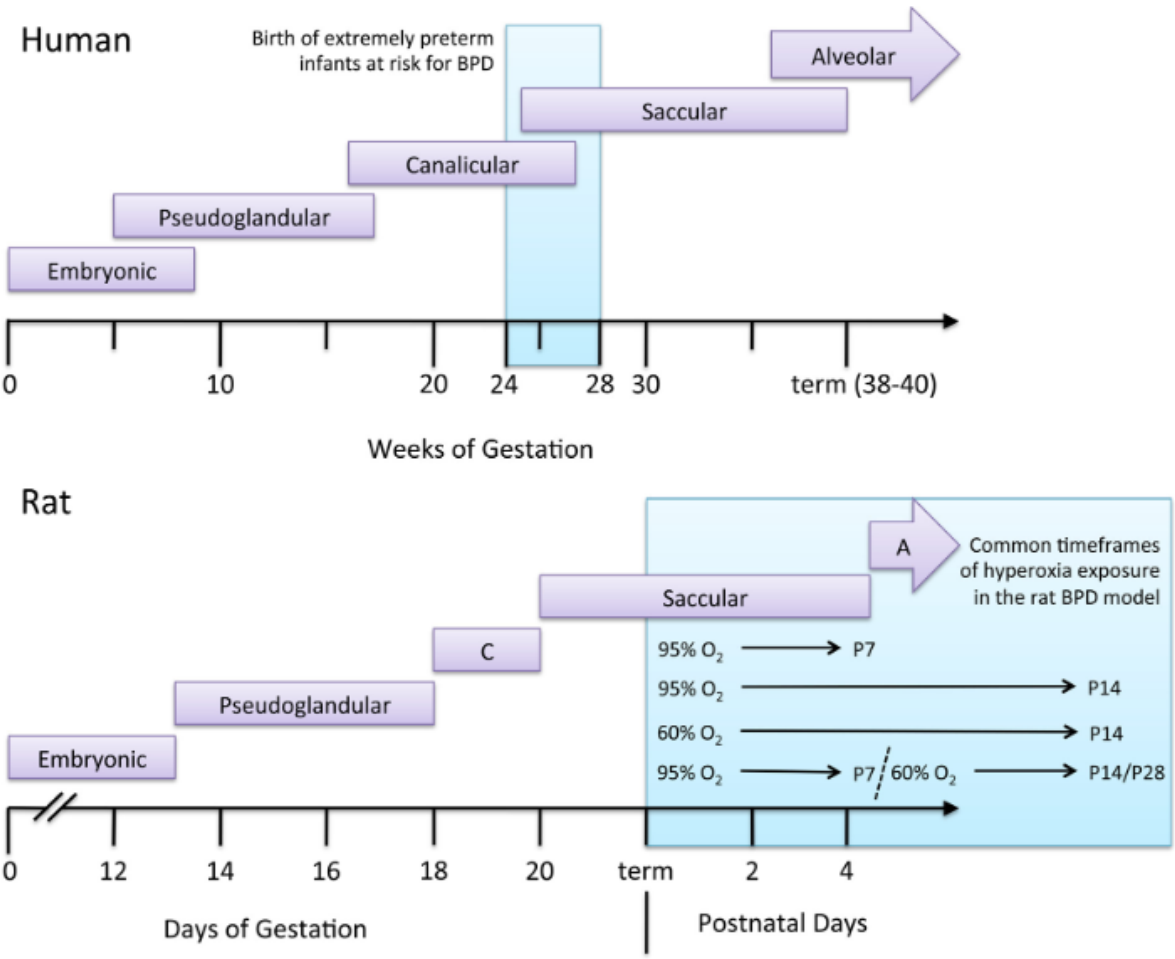

Figure 5. Rats are born at a lung developmental stage similar to that of preterm infants. Preterm infants at risk of developing BPD are born between the late-canalicular to early-saccular phase of lung development. Rats are born in the saccular phase of lung development whereas the alveolar phase occurs postnatally. Common timeframes of hyperoxia exposure are initiated at birth and continue to the alveolar phase to produce experimental models of BPD. A, alveolar; C, canalicular; P, postnatal day. Ref 27.

1.2 Stem cell therapies for BPD

1.2.1 Stem cells

Stem cells have the capability of differentiating into different types of cells and can also renew themselves over a long period of time. There are three main types of stem cells: 1) embryonic stem cells (ESCs), 2) induced pluripotent stem cells (iPSCs) and 3) adult stem cells.

ESCs are found in the inner cell mass in an early embryo. They are pluripotent, meaning they can differentiate into any cell type in the body. iPSCs are also pluripotent cells created by reprogramming adult cells using the Yamanaka factors, Oct4, Sox2, Klf4, and c-Myc, into an embryonic stem cell-like state. Adult stem cells such as mesenchymal stromal cells (MSCs) and hematopoietic stem cells (HSCs) are multipotent, meaning they can differentiate into several cell types, but not all or they are unipotent (they can differentiate into one cell type only). MSCs can differentiate into osteoblasts, chondrocytes and adipocytes whereas HSCs can differentiate to all types of blood cells (30,31).

1.2.2 Mesenchymal Stromal Cells (MSCs)

MSCs have anti-inflammatory, immunomodulatory and regenerative properties (32). Their multimodal mechanisms of action make them an attractive therapeutic candidate for multifactorial diseases such as BPD. MSCs can be isolated from the bone marrow (BM), adipose tissue, umbilical cord (UC), UC blood, placenta, and amniotic fluid. Given that there are several ways to isolate MSCs from multiple human tissues, the International Society for Cell and Gene Therapy (ISCT) developed minimal criteria to identify MSCs: they must 1) adhere to plastic, 2) display specific cell surface marker profiles identified by flow cytometry (CD73+, CD90+, CD105+, CD34-, CD45-, CD14/CD11b-, CD79α/CD19-, HLA-DR-), and 3) differentiate into osteoblasts, adipocytes, and chondrocytes (33).

UCs are a clinically relevant source of MSCs as they allow for a non-invasive collection of MSCs. UC-MSCs have unique advantages such as being highly proliferative, easily accessible and possessing low immunogenicity (34). Preclinical trials have shown that UC-MSCs have the potential to regenerate damaged organs (35). In addition, early phase clinical trials have shown the safety and feasibility of MSCs in preterm infants (36).

1.2.3 MSCs properties and mechanisms of action

MSCs were first recognized for their immunomodulatory properties when they were discovered to suppress allogeneic T cell response and prevent the formation natural killer (NK) cells (37). The immunomodulatory properties of MSCs have been attributed to their secreted products. Some of the top efficient ones include indoleamine 2,3-dioxygenase (IDO), prostaglandin-E2 (PGE2), nitric oxide (NO), transforming growth factor (TGF)-β1 and interleukin (IL)-10 (38–41). IDO is a rate-limiting enzyme in the tryptophan catabolic pathway which is often considered a potency marker for MSCs' immunomodulatory properties as MSCs have been shown to suppress T cell activation in an IDO-dependent manner (42).

In addition, MSCs are also recognized for their regenerative properties due to their secretion of growth factors such as vascular endothelial growth factor (VEGF), hepatocyte growth factor and TGF. MSCs also secrete cytokines and chemokines such as monocyte chemoattractant protein 1 (MCP-1) and granulocyte-macrophage colony-stimulating factor (GM-CSF) which are necessary for inhibiting cellular apoptosis and restoring tissue homeostasis (43). Furthermore, evidence shows that MSCs transfer their mitochondria to alveolar cells in an acute lung injury model while other studies show that MSCs induce M1 to M2 macrophage polarization **(Figure 6)** (44–46).

MSCs are also known for releasing paracrine factors and bioactive molecules such as cytokines and extracellular vesicles (EVs) which have anti-inflammatory and anti-fibrotic capacities (47,48). EVs are membrane vesicles, ranging from 40 nm to a few μm in size, which contain enzymes, cytokines, growth factors and mRNA (48). EVs mediate cell-to-cell communication by transferring their bioactive payload and/or binding with receptors, lipids and glycans to contribute to physiological and pathophysiological changes of recipient cells (49,50).

EVs between 40-150 nm in size, known as exosomes, originate from the endocytic pathway and are surrounded by a lipid bilayer (51).

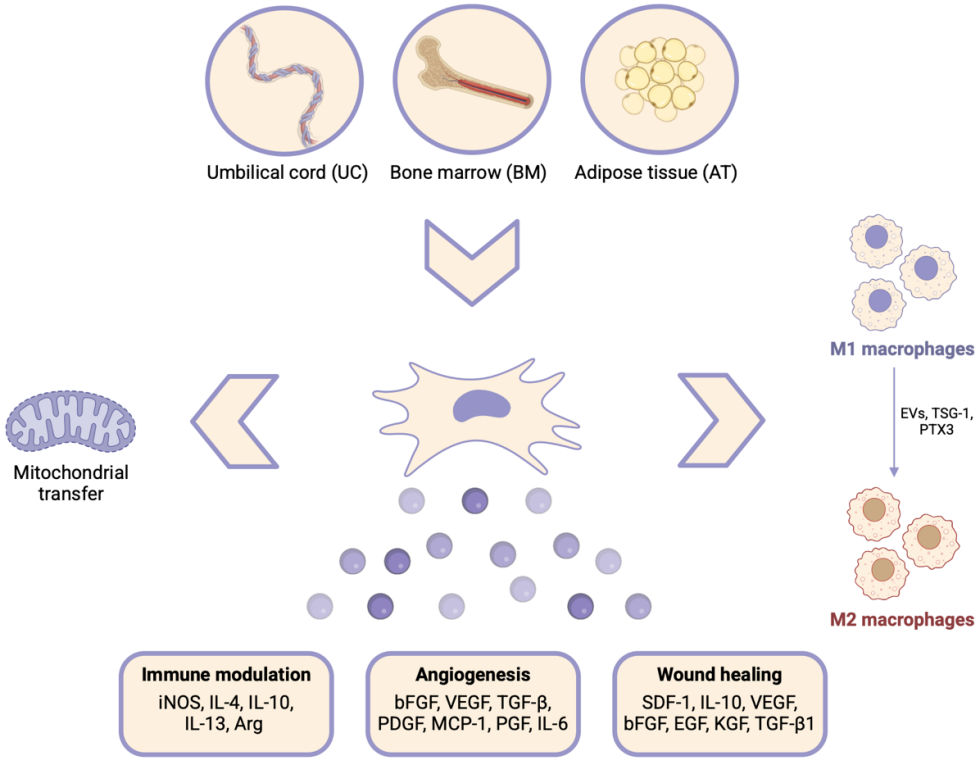

Figure 6. Suggested therapeutic functions of mesenchymal stromal cells (MSCs). MSCs can be isolated from a variety of tissue. MSCs have the ability to transfer their mitochondria to pulmonary alveoli to protect against acute lung injury. MSCs have also been shown to induce M1 to M2 polarization. The secretome of MSCs is known to be involved in immune modulation, wound healing and angiogenesis. Figure adapted from Ref 43 and 44 and made with Biorender.

1.2.4 MSCs therapeutic effects in experimental BPD

Experimental studies in animal models of BPD indicate that MSCs offer lung-protective effects. MSCs significantly improved alveolarization, PH, lung inflammation, fibrosis, angiogenesis, and apoptosis (52). Common sources of MSCs include the BM, UC and UC blood. Routes of administration included I.V., I.T., intraperitoneal (I.P.) and intranasal (I.N.) routes.

1.2.5 MSC EVs as an alternative treatment to their parent cells

As previously described, the therapeutic effect of MSCs is most likely due to their paracrine activity rather than their engraftment and differentiation in injured tissue. Increasing data supports the notion that EVs could substitute their parental cells in regenerative medicine. In fact, EVs have several advantages compared to their parent cells. First, EVs are less likely to trigger an immune response due to their lower immunogenicity and transmembrane proteins on their surface (53). Second, EVs are safe because they are rapidly cleared *in vivo* (54). Third, they cannot form tumors because of their inability to self-replicate. Finally, they can be constantly released by one immortalized cell line, defying the problem of small-manufacturing due to prolonged cell culture times and low amounts of isolated cells (55).

Therefore, several preclinical studies have explored the effect of MSC EVs in lung injury animal models, specifically small EVs, a class of EVs which includes exosomes (56). For example, Willis et al. demonstrated that MSC EVs restored lung structure, reduced pulmonary fibrosis, ameliorated PH and improved exercise capacity in a neonatal murine hyperoxia-induced lung injury model (57). The same group started a clinical trial to investigate the therapeutic effect of MSC EVs on patients with BPD, however, this trial was halted by the sponsor due to business rather than safety concerns (clinicaltrials.gov Identifier: NCT03857841). Nevertheless, this attempt highlights how close the field is to bringing MSC EVs therapies into the clinic.

Only small clinical studies are ongoing to test MSC EVs, which means that more clinical trials need to be done to know if MSC EVs are effective in treating inflammatory and pulmonary diseases. Currently, several clinical studies are investigating the effect of MSC EVs on inflammatory/immune diseases (58,59). In a study by Kordelas et al., a patient with therapy-refractory graft-versus-host disease (GvHD) received four doses of MSC EVs. MSC EVs

administration reduced pro-inflammatory cytokine response of the patient's PBMCs and significantly improved clinical symptoms of GvHD such as diarrhea and mucosal GvHD within two weeks following treatment (60). In another study, by Sengupta and colleagues, 24 patients with SARS-CoV-2-associated respiratory distress syndrome received MSC EVs. Following MSC EV therapy, the patients had restored oxygenation, reduced inflammation and improved immunocompetence (61). Although these are small studies, they highlight that MSC EVs may provide a new safe tool to treat inflammation-associated diseases.

1.2.6 Current challenges in MSC and MSC EV therapy for BPD

While more than 1,000 clinical trials have tested MSCs in a range of diseases, only three Phase III clinical trials have been completed and published so far on GvHD and Crohn's disease and only one MSC product (OSSM-001) received FDA approval to treat perianal fistulizing Crohn's disease (62,63). This sheds light on the variability in clinical outcomes which are attributed to the variability in MSCs themselves. Although the ISCT minimal criteria helps eliminate contaminant cells such as hematopoietic and endothelial cells, leukocytes, monocytes, macrophages and B cells, they do not guarantee that the cells are therapeutic. In addition, it has been recognized that *in vitro* expanded MSC populations are inherently heterogeneous as they are diverse in morphology and proliferation rates leading to cell-to-cell variation (64). Furthermore, heterogeneities exist in MSCs isolated from different donors, tissues and clones (65). A recent study shows that heterogeneity in tissue-derived MSCs impacts their proliferation, differentiation, immunophenotype and secretome (66). For example, it has been shown that UC-MSCs are superior to BM-MSCs in their proliferation potential, lower immunogenicity, higher differentiation abilities and their non-invasive method of isolation (67). Therefore, standardizing MSC populations is an important consideration in clinical applications as their heterogeneity could explain inconsistent

results in clinical trials (68). Our lab has attempted to find a subpopulation of MSCs that has superior therapeutic efficacy. Single-cell RNA sequencing identified UC-MSCs with a unique progenitor transcriptome with lung protective effects, while UC-MSCs with a fibrotic transcriptome had no therapeutic benefit (69). Furthermore, UC-MSCs expressing high levels of human leukocyte antigen (HLA)-A, -B, and -C show reduced therapeutic effect in a hyperoxia-induced lung injury rat model (69)

On the other hand, although EVs offer exciting benefits when compared to their parental cells, their production in large quantities remains a limiting factor when it comes to clinical applications, especially considering that the expansion of MSCs is limited in culture. Scalable EV isolation methods are required to support preclinical and clinical demands. In preclinical studies, a dose of 10^9-10^{10} EVs per mouse is required to achieve biological outcomes (70–73). Therefore, several months are required to harvest the required volume of conditioned media (CdM) before processing it to support a well-powered animal study.

Differential ultracentrifugation (dUC) is the most employed method to isolate EVs (74). It mainly requires spinning the UC-MSC CdM at 20,000g to remove dead cells, apoptotic bodies and microvesicles, followed by another spin at 100,000g to pellet the EVs. Due to requiring multiple centrifugation steps with limited volumes of CdM per spin, this method is not a cost-effective strategy for scale-up. On the other hand, tangential flow filtration (TFF) is a scalable strategy often used to concentrate proteins and viruses from large amounts of CdM (75–77). TFF requires spinning the CdM at 20,000g before circulating it parallel to a filter, allowing unwanted particles to pass through the membrane. This method concentrates the CdM around 10 times which increases the feasibility of spinning the concentrated CdM at 100,000g to pellet the EVs.

Ultimately, it is important to acknowledge the challenges that should be addressed regarding the use of EV-based therapies in the clinic. This includes testing their half-life, optimal dose and endocytosis capacity by other cells. In addition, it is important to use cGMP procedures that yield EVs with high recovery, purity, potency, and sterility. Finally, the biodistribution of EVs is crucial to help determine their localization (78).

1.3 iPSC-derived MSCs (iMSCs) and their potential of becoming new candidates of cell therapy

iMSCs present a novel opportunity to overcome challenges associated with translating MSC therapies to the clinic **(Table 1)** (79). iMSCs minimize the diversity associated with using tissue-derived MSCs. mRNA reprogramming technology offers a safe, non-viral and genomic-integration-free strategy to introduce transcription factors that transform somatic cells to iPSCs, providing a promising route for clinical applications **(Figure 7)**. iPSCs are then differentiated into MSCs using various protocols such as MSC Switch, Embryoid Body Formation, Specific Differentiation, Pathway Inhibitor, and Platelet Lysate (80). Advancements in genome-engineering have unlocked additional avenues to ensure the safety and efficacy of iMSCs. These strategies will be explored in section 1.3.2.

Table 1. Summary of advantages and disadvantages of iMSCs compared to tissue-derived MSCs. Adapted from Ref 74 and 75.

Advantages of iMSCs	Disadvantages of iMSCs
Well-established gene editing protocols for iPSCs allow for integrating therapeutic genes	iPSCs should be generated using micro-RNA or plasmids rather than viral-based methods to ensure iMSC safety
Lower immunogenicity and avoiding ethical restrictions	Requires standardization of iMSC generation protocols to ensure homogeneity between different products
Being more homogeneous/uniform than traditional MSCs due to unlimited and consistent source of starting material	Early stage of industrialization
Scalable production and stable quality	High costs and technical requirements
Minimally invasive procedure for collecting iPSC starting material	

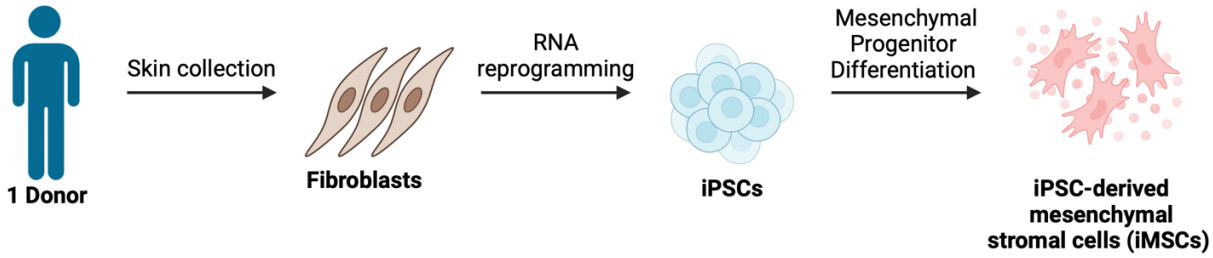

Figure 7. An example of the iMSC manufacturing process. Fibroblasts are collected from a healthy donor and are reprogrammed to iPSCs using RNA reprogramming technology. iPSCs are further differentiated to MSCs (iMSCs). Figure adapted from Ref 84 and made with Biorender.

1.3.1 Applications of iMSCs and iMSC EVs in preclinical disease models

Evidence suggests that iMSCs primarily cause strong immunomodulatory effects. One study shows that iMSCs inhibit T cell proliferation, reduce Th1, Th2 responses and upregulate the

Treg response (81). Another group showed that iMSCs prevent the differentiation and proliferation of cytotoxic CD8 T cells into Type 1 cytotoxic T cells (82). In addition, iMSCs have been shown to downregulate ERK1/2 signalling pathway, suppressing the cytolytic function of NK cells (83).

Most preclinical studies testing iMSCs fall into these three categories: 1) inflammatory diseases, 2) cancer, and 3) GvHD. Regarding inflammatory diseases, iMSCs have been shown to significantly dampen inflammation, promote angiogenesis and restore microbial composition in mice subjected to chemically induced small intestine-colon inflammation to mimic inflammatory bowel disease (84). On the other hand, iMSCs have shown strong anti-tumor effects in a study where iMSCs with *IL-24* transgene integration restrained melanoma growth in a melanoma mice model (85). As for applications in GvHD, an investigation showed that iMSCs with a low dose of Rapamycin facilitated immune tolerance in diabetic mice receiving islet transplantation by suppressing Th1 and enhancing Treg cells differentiation (86). Furthermore, iMSCs have also shown great potential in treating airway inflammation by improving airway remodelling and decreasing pulmonary fibrosis through their superior immunomodulatory capacities. TGF-β1 Smad2/Smad3 signaling pathway was suggested as the mechanism involved in mediating these effects (87).

There are a substantial number of studies which tested iMSC EVs in preclinical disease models. They were shown to be as good or sometimes better than tissue-derived MSCs (79). These models range from inflammatory and autoimmune diseases to vascularization and tissue regeneration. In asthma and allergic rhinitis, iMSC EVs were reported to significantly reduce inflammatory cells such as eosinophils and neutrophils through the high expression of miR-146a-5p, causing a decrease in Group 2 innate lymphoid cells (ILC2s) which are believed to play a critical role in these diseases (88). In addition, subcutaneous injections of iMSCs EVs promoted

re-epithelialization, scar reduction and increased blood vessel formation in a rat wound model (89). Another study demonstrated that iMSC EVs showed promise in promoting angiogenesis under ischemic conditions (79). An intramuscular injection of iMSC EVs restored the microvessel structure in a mouse model of limb ischemia (90). Similarly, in a rat stroke model induced by middle cerebral artery occlusion, iMSC EVs improved angiogenesis and neurological outcomes (91). iMSC EVs have also shown strong tissue regenerative capacities in corneal disease models where they repaired damaged corneal epithelium and reduced scarring and collagen expression (92).

1.3.2 Technological advancements to ensure the safety of iMSCs for clinical translation

Methods to improve the safety of iMSCs include the use of transcriptional links between a drug-inducible suicide gene (herpes simplex virus thymidine kinase (HSV-TK) and a cell-division gene (CDK1) to ensure the absence of residual undifferentiated iPSCs. This suicide gene is inducible by ganciclovir, an FDA-approved antiviral prodrug (93).

Other methods to ensure the removal of residual iPSCs include culturing the differentiated cells in single-cell suspension in a semi-solid medium followed by adherent culture conditions which do not support iPSC survival, allowing only the survival of iMSCs (94). Furthermore, assays have been developed to measure the expression of LIN28 gene, associated with the pluripotent stem cell fate (94). This has been accompanied by an in vitro tumorigenicity assay to detect the potential presence of iPSCs capable of colony formation in soft agar. In fact, these methods have been used by Cynata Therapeutics, an Australian stem cell and regenerative medicine company, which supplied iMSCs (CYP-001) to the first clinical trial of iPSC-derived cells in any disease

(94). In this phase 1 clinical trial (no. NCT02923375), patients with steroid-resistant (SR)-aGvHD received an intravenous infusion of iMSCs. Day 28 overall response rates (often used as a primary efficacy endpoint) ranged from 62.5% (low dose) and 87.5% (high dose). In comparison, day 28 overall response rates in SR-aGvHD patients treated with BM-MSCs ranged from 45% to 86.5% (95). Two years later, the investigators reported two-year safety outcomes. The two-year survival rate was 60% in patients treated with iMSCs whereas patients treated with BM-MSCs in another study reported a two-year survival rate of 22% to 39% (96). Causes of death were unrelated to CYP-001 treatment. In addition, there were no serious adverse events, tumors or other safety concerns related to CYP-001. This trial underscores the safety of iMSCs due to the strategies used, paving the way for further clinical trials of this kind.

1.3.2 Clinical evidence of iMSC therapeutic efficacy

As of January 2025, there are 116 registered clinical trials that use human pluripotent stem cell (hPSC)- derived products (97). In fact, more than 1,200 patients worldwide received hPSC-derived products, and no safety concerns have been reported so far. These clinical trials mainly targeted the eye, central nervous system, and cancer. Only six of those clinical trials utilized iMSCs, whereas seven utilized hESC-derived MSCs. Five of those are completed phase I clinical trials.

In addition to the completed CYP-001 phase I trial (no. NCT02923375) mentioned above, Cynata Therapeutics helped complete another phase I trial to test intravenous infusions of CYP-001 in patients with COVID-19 (no. NCT04537351). Their rationale was that iMSCs would provide powerful anti-inflammatory and immune-suppressive effects which would dampen inflammation in the lungs. However, results from this study are not yet reported. Similarly, a group from Wuhan Jinyinyan Hospital completed a phase I clinical trial for testing iMSCs in patients

with COVID-19 (no. ChiCTR2000031139), but the results are not yet reported. Another completed phase I clinical trial tested hESC-MSCs in patients with interstitial cystitis (no. NCT04610359) and reported that although the patients showed improvement in pain and lesion size, the sample size was too small to reach any conclusions. The last completed phase I clinical trial tested hESC-MSCs in patients with primary ovarian insufficiency (no. NCT03877471) but did not release any results yet.

It is worth mentioning that a placebo-controlled, double-blinded phase III clinical trial is underway to test iMSCs supplied by Cynata Therapeutics (CYP-004) in patients with osteoarthritis (no. ACTRN12620000870954). So far, they reached the target sample size of 320 patients, but the data is yet to be released. This would be the first phase III trial to be conducted with hPSC-derived products, rendering its results to be critical for this field.

Overall, the evidence so far suggests that iPSC-derived cell therapies are safe (97). Thus, it is important to further explore iMSCs as a potentially more optimized cell therapy that overcomes donor-to-donor variability, enhancing their therapeutic potential.

2. Rationale, hypothesis and aims

2.1 Rationale

BPD is the most common and severe lifelong complication of extreme prematurity with no cure. It is characterized by an arrest in alveolar and vascular growth. Exposure to hyperoxia and inflammation is associated with the development of BPD. MSCs are multi-potent cells with anti-inflammatory, immunomodulatory and regenerative properties. We have previously reported that UC-MSCs isolated from distinct donors offer different therapeutic potential in experimental BPD. Therefore, MSC populations standardization is an important aspect to achieve in clinical applications as their heterogeneity may lead to inconsistent results in clinical trials.

2.2 Hypothesis

We hypothesize that iPSCs offer a more uniform source of MSCs, providing a more homogenous effect when compared to UC-MSCs.

2.3 Aims

In this context, the main aims of this project were:

1) To explore the heterogeneity of UC-MSCs derived from different donors in hyperoxia-induced lung injury in neonatal rats.
2) To characterize iMSCs and UC-MSCs using flow cytometry.
3) To assess the therapeutic potential of UC-MSCs and iMSCs in hyperoxia-induced lung injury in neonatal rats.

3. Materials and methods

3.1 Ethics approval

Human Research Ethics Board (Ottawa, Canada) and "Ethikkommission der Technischen Universität Dresden" (Dresden, Germany) approved human samples collection. Animal Care Committee of the University of Ottawa (OHRI-3151) approved animal experiments.

3.2 UC-MSCs isolation

Following informed consent from the parents, UC-MSCs were isolated from the UC of a healthy term pregnancy as previously described (98).

3.3 Animal model

Pregnant Sprague Dawley rats (Charles Rivers, Saint Constant, QC, Canada) were ordered. At postnatal day 0 (P0), pups were pooled and randomized to obtain equal litter size of 12 pups per dam. The dam and their litter were either exposed to room air (RA- 21% O_2) or lung injury (85-90% O_2) from P0 to P14 (sealed plexiglass chambers with continuous oxygen monitoring [BioSpherix, Redfield, NY]). Three RA cages and three O_2 cages were used to have enough dams to rotate O_2 to RA-exposed dams every 48 hours to avoid oxygen toxicity. However, only one RA cage was used for analysis as a control group. At P21, the animals were euthanized by intraperitoneal (I.P.) injection of pentobarbital sodium (Euthanyl, 0.2 mL, 65 mg/mL).

3.4 UC-MSC preparation for *in vivo* administration

Passage two to three UC-MSCs were plated as previously described and placed for 24 to 72 hours in a cell culture incubator at 37°C with 5% CO_2 and 5% O_2 (98). Trypsinization of cells

was performed using TrypLE (cat#12605028, ThermoFisher Scientific, Waltham, MA, USA), then cells were counted, washed, and resuspended in 1XPBS at a concentration of 4,000 cells/µl, such that a 30µl dose contained 120,000 cells (dose: 10,000,000 cells/kg body weight). At P4, pups were anesthetized by inhalation of 5% isoflurane, then maintained with 3% isoflurane, in a mixture of 100% O2 at 1.5 L/min. Surgery was performed to expose the trachea. Either 30µl of 1XPBS or UC-MSCs in 1XPBS were administered intratracheally (I.T.).

UC-MSC donor information:

Donor	Year of isolation	Geographic location of recruitment	Gestational age (*wk* + *d*)	Birth weight (g)	Sex	Maternal age (yr)	Delivery	Surface markers (ISCT criteria)	Tri-lineage differentiation
1	2020	Germany	39 + 1	3510	Female	34	Cesarean section	Yes	Yes
2	2023	Canada	39 + 3	3520	Female	39	Cesarean section	Yes	N/A
3	2023	Canada	N/A	N/A	N/A	N/A	N/A	Yes	N/A
4	2020	Germany	37 + 3	3320	Female	33	Cesarean section	Yes	Yes
5	2021	Germany	36 + 6	3205	Male	42	Cesarean section	Yes	Yes
6	2023	Canada	39 + 0	3510	Male	35	Cesarean section	Yes	Yes

3.5 UC-MSC CdM collection for UC-MSC EVs isolation

Passage three UC-MSCs were plated in 15cm dishes with EV-depleted FBS (Thermo Fisher catalog #A2720801) culture media and expanded till passage five with a constant seeding density of 1 million cells per 15cm dish. Every two days, the CdM was collected in an even number of Falcon tubes and stored in the -80°C freezer and fresh media was added to the dishes. Once the cells reached 80-90% confluency, the CdM was collected as described above and the cells were split into new 15cm dishes (1 million cells/15cm dish) until they reach passage 5. At each cell splitting stage, the number of cells was counted towards cell equivalence. During media changes,

the number of cells seeded was used to calculate cell equivalence. To summarize, half of the total MSC CdM collected was used for TFF EV isolation and the other half was used for UC EV isolation (29 million cells per technique).

3.6 Isolating UC-MSC EVs using tangential flow filtration (TFF)

400mL of MSC CdM in EV-depleted FBS generated from 29 million cells were centrifuged at 20,000g for 20 minutes at 20°C to remove dead cells, apoptotic bodies and microvesicles. Next, the supernatant was collected and run through the 300kDa TFF cartridge at 39mL/min until the sample was 10x concentrated. This process took approximately 2 hours. Once the CdM was concentrated 10x, diafiltration took place; a buffer exchange strategy to wash the sample with PBS at 10mL/min until the CdM becomes nearly transparent. Next, the CdM was centrifuged at 100,000g for 90 minutes at 4°C to pellet the EVs. Finally, the EV pellet was resuspended in particle-free PBS to obtain a dose of 2.14 million cell equivalents per 30µl to achieve a dose of 143 million cell equivalents/Kg. This dose was calculated based on a previous study which showed a therapeutic effect of TFF-derived MSC EVs in a hyperoxia-induced lung injury model in neonatal mice (57).

3.7 Isolating UC-MSC EVs using differential ultracentrifugation (dUC)

400mL of MSC CdM in EV-depleted FBS generated from 28.436 million cells were centrifuged at 20,000g for 20 minutes at 20°C using 50mL polycarbonate tubes and type JA25.5 rotor (Beckman Coulter, Avanti J-26 XPI) to remove dead cells, apoptotic bodies and microvesicles. Next, the supernatant was collected and centrifuged at 100,000g using 26.3mL polycarbonate tubes and type 70Ti rotor (Beckman Coulter, OptimaTM XE) for 90 minutes at 4°C to pellet the EVs. The resulting pellets from individual 26.3mL polycarbonate tubes from 70Ti

rotor were pooled into a single 10.4mL polycarbonate tube and centrifuged in a 70.1Ti rotor (Beckman Coulter, OptimaTM XE) at 100,000g for 90 minutes at 4°C to obtain the final MSC EV pellet. Finally, the EV pellet was resuspended in particle-free sterile PBS to obtain a dose of 2.14 million cell equivalent per 30µl to achieve a dose of 143 million cell equivalents/Kg.

3.8 Characterizing UC-MSC EVs using nanoparticle tracking analysis (NTA)

UC-MSC-derived particles distribution and concentration were measured using nanoparticle tracking analysis (ZetaView® Nanoparticle Tracking Analyser). The dUC sample was diluted 1:1000 in EV-depleted PBS whereas the TFF sample was diluted in 1:8000 in EV-depleted PBS. Next, the samples are manually injected into the instrument, and videos were acquired at ambient temperature per sample.

3.9 Characterizing UC-MSC EVs using the Bradford assay for protein quantification

After resuspending the MSC EV pellets generated from TFF and UC in EV-depleted PBS, 20µl aliquots are kept aside and diluted 1:5 in EV-depleted PBS for protein quantification. Eight standards of bovine serum albumin (BSA) by Bio-Rd were used to cover the linear range of a Bradford protein assay, ranging from 0.125 to 2 mg/ml. Next, 10 µL of each standard and sample were added to a 96 well-plate followed by 250 µL of diluted (1:5) Bio-Rad Coomassie Brilliant Blue (G-250) Protein Reagent in each well. Proteins in each sample bind to the reagent and undergo a color change in the visible spectrum with the absorbance maximum moving from 470 to 595 nm, which is directly proportional to the amount of protein per sample. The absorbance at 595 nm is read by a microplate reader (Biotek). The exact protein concentration per sample is

determined by interpolation from a standard curve made by measuring the absorbance of a dilution series of protein standards of known concentrations within the linear response range of the assay.

3.10 iMSC preparation for *in vivo* administration

Passage one iMSCs obtained from Pluristyx were plated and placed for a week in a cell culture incubator at 37°C with 5% CO_2 and 21% O_2. Next, the iMSCs were either injected (first two experiments) or passaged one more time (third experiment) before injections. Cells were dissociated using Accutase (cat#07920, STEMCELL Technologies), then cells were counted, washed, and resuspended in 1XPBS at a concentration of 4,000 cells/µl, such that a 30µl dose contained 120,000 cells (dose: 10,000,000 cells/kg body weight). At P4, pups were anesthetized by inhalation of 5% isoflurane, then maintained with 3% isoflurane, in a mixture of 100% O2 at 1.5 L/min. Surgery was performed to expose the trachea. Either 30µl of 1XPBS or UC-MSCs in 1XPBS were administered intratracheally (I.T.).

3.11 Characterizing UC-MSCs and iMSCs using flow cytometry

The BD Stemflow™ Human MSC Analysis Kit (562245, BD Biosciences, USA) was used to analyze the panel proposed by ISCT (99). UC-MSCs were used as a positive control and ECFCs were used as a negative control for CD90. DAPI was included to measure viability.

3.12 Cell potency assay using Indoleamine 2,3-dioxygenase (IDO) qPCR

UC-MSCs were thawed in a 37°C water bath for one minute, diluted in complete media (DMEM containing platelet lysate and glutamine) and divided into two 15mL conical tubes. One of the two cell suspensions was treated with 20 ng/mL of IFN-γ while the other remained untreated as a control. Each cell suspension was seeded into a separate T75 flask at various seeding densities

(See table below). Cells were cultured at 37°C with 5% O2 and 5% CO2 for 24 hours. For harvest, flasks were washed with 7 mL of PBS and then coated with 1 mL of PBS. Cells were detached with a cell scraper and transferred to microcentrifuge tubes. Cells were centrifuged at 17,000 x g for 1 minute, the supernatant discarded, and pellets stored at -80°C until RNA extraction. Total RNA was prepared from cell lysates with QIAGEN RNeasy kit (Cat# 74104) and converted to cDNA using QIAGEN QuantiTect Reverse Transcription kit (Cat# 205311). Quantitative PCR (qPCR) was performed with validated primers, QIAGEN QuantiTect Primer Assays (Cat# QT00000504 (IDO), QT00079247 (GAPDH)) using QIAGEN QuantiTect SYBR Green PCR kit (Cat# 204143) according to manufacturer's instructions. The expression level of IDO RNA was determined based on the relative quantification cycle (Cq) values for IDO normalized to endogenous control gene GAPDH. The fold induction of IDO in samples from IFNγ-treated cells (IFNγ+) vs. untreated cells (IFNγ-) was calculated using the Delta-delta Cq method as follows:

Relative fold gene expression $= 2^{-\Delta\Delta Cq}$

$$\Delta\Delta Cq = \left(\left(avgCq\ IDO_{(IFNy+)} - avgCq\ GAPDH_{(IFNy+)}\right) - \left(avgCq\ IDO_{(IFNy-)} - avgCq\ GAPDH_{(IFNy-)}\right)\right)$$

Cell culture and IFNγ treatment schedule:

Sample ID	Seeding density (cells/cm2)	IFNγ treatment (start time and date)	IFNγ treatment (end time and date)
Donor 4	33 000	13:52/26-MAR-2025	14:13/27-MAR-2025
Donor 5	46 000	14:15/26-MAR-2025	14:32/27-MAR-2025
Donor 6	40 000	14:40/26-MAR-2025	14:48/27-MAR-2025
iMSCs	12 000	15:00/24-MAR-2025	15:00/25-MAR-2025

3.13 Echocardiography

As previously described, echocardiography is done at P19 (69). 5% isoflurane (in 100% O_2 at 1.5 L/min) was used to anesthetize the pups, followed by 3% isoflurane to maintain

anesthesia. A Pulsed-wave Doppler of pulmonary outflow was used to obtain echocardiography images. These images were used to measure pulmonary arterial acceleration time (PAAT) and pulmonary arterial ejection time (PAET). PAAT is the interval between the onset of the systolic pulmonary arterial flow and peak flow velocity. PAET is the interval between the onset of pulmonary arterial flow to the end. The PAAT/PAET ratio was calculated as a proxy of PH.

3.14 Lung function tests

At P21, a tracheostomy was performed, and lung function (pressure volume [PV] loop) was assessed using FlexiVent (SCIREQ, Montreal, QC, Canada) as previously described (100). The results were normalized with the body weight (g) of the animals for comparison.

3.15 Fulton's index

The hearts were harvested, and the right ventricle was separated from the left ventricle and septal wall. The heart tissue was left to dry. Three days later, the weight of the right ventricle to the left ventricle + septum ratio (RV/LV+S) was calculated as an index of right ventricular hypertrophy (RVH).

3.16 Lung histology and structure analysis

Following harvest, the right lungs were flash frozen in liquid nitrogen and stored in a -80°C freezer. The left lungs were inflated and fixed through the trachea with 10% buffered formalin (cat#SF100-4, Fisher Scientific, Fair Lawn, NJ, USA) at a constant pressure of 20cmH_2O. The trachea was then removed, and the lungs were fixed for 48 hours in 10% buffered formalin (cat#SF100-4, Fisher Scientific, Fair Lawn, NJ, USA) at room temperature (RT). Next, the lungs were emersed in paraffin, cut into 4µm-thick serial sections, and stained with hematoxylin and

eosin (H&E) by the Louise Pelletier Histology Core Facility at the University of Ottawa. Alveolar size was quantified by a motorized microscope stage, using the mean linear intercept (MLI) estimation at a magnification of 20X as described earlier (69).

3.17 Statistical analyses

All statistical analyses were performed using GraphPad Prism 9.0. Values are represented as the mean ± SD. P values were calculated using the unpaired, two-tailed *t* test, one-way ANOVA, or the log-rank (Mantel-Cox) test (for Kaplan-Meier curves), and P values ≤ 0.05 were considered to indicate statistical significance. Endpoints with three groups or more were compared using one-way ANOVA. When one-way ANOVA showed significance, we used Tukey's multiple-comparison *post hoc* test (used to compare the effects of each group with each other to determine which treatments were better/worse). All group assignments were blinded before analysis.

4. Results

4.1 Treatment with UC-MSCs isolated from Donor 1, but not Donor 2 or 3, improved lung function in a hyperoxia-induced rat BPD model.

Our aim in this experiment was to identify a therapeutic donor of UC-MSCs to use for isolating and testing EVs in subsequent experiments. UC-MSCs isolated from Donor 1, 2 and 3 were tested for their therapeutic potential in a hyperoxia-induced lung injury model in neonatal rats. Rat pups were exposed to hyperoxia (85% O_2) from birth at postnatal day 0 (P0) to P14 and kept in room air until P21 **(Figure 8A)**. UC-MSCs were administered during the saccular stage of lung development in neonatal rats at P4, corresponding to the stage at which preterm infants who develop BPD are born **(Figure 8A)**. No significant differences in survival were observed in all groups **(Figure 8B)**. Pressure-volume (PV)-loop FlexiVent measurement was used to assess lung function **(Figure 8C)**. A significant decrease in delivery volume at 30 cmH_2O (peak pressure) was observed in the lung injury PBS group, indicating a strong disease model **(Figure 8D**). UC-MSCs from Donor 1, but not Donor 2 and 3, restored lung function **(Figure 8D)**. Lung injury significantly increased the Fulton's index (right ventricular hypertrophy, RVH) **(Figure 8E)**. However, none of the UC-MSCs were able to decrease RVH **(Figure 8E)**.

In summary, this experiment identifies Donor 1 as a therapeutic UC-MSC donor and highlights the heterogeneity of UC-MSCs isolated from different donors.

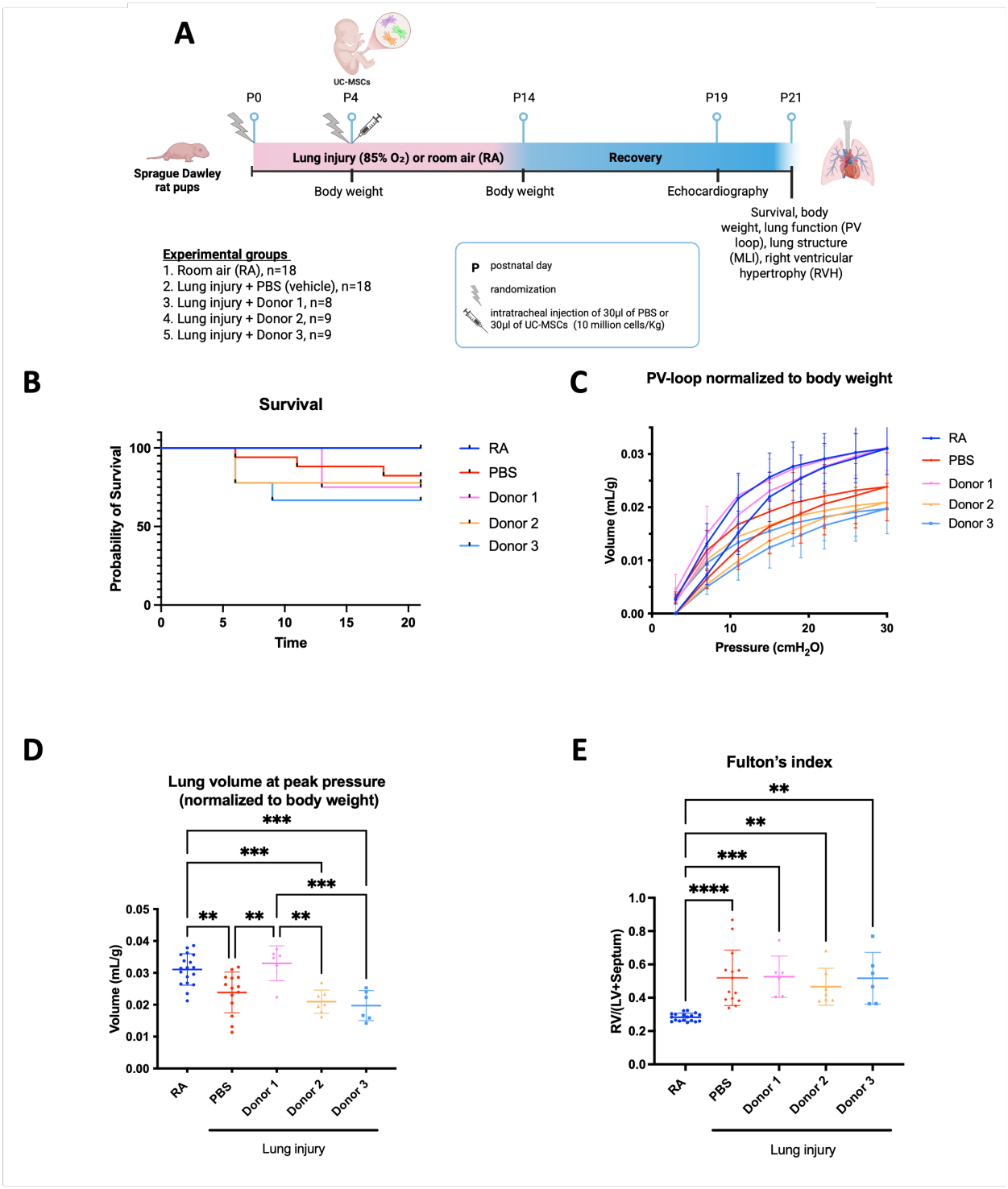

Figure 8. Treatment with UC-MSCs isolated from Donor 1, but not Donor 2 and 3, improved lung function in a hyperoxia-induced rat BPD model. A) Schematic representation of the hyperoxia-induced lung injury model in neonatal rats as well as timelines for injections and endpoints. **(B)** Survival rate (%) on postnatal day 21. **(C)** Body weight-adjusted pressure volume (PV)-loops curves where each loop represents the mean lung volume of all pups within one group at each pressure point (RA untreated; n=18, O2 + PBS; n=14, Donor 1; n=6 and O2 + Donor 2;

n=6, Donor 3; n=6). **(D)** Body weight-adjusted inspiratory capacity (mL/g) (RA untreated; n=18, O2 + PBS; n=14, Donor 1; n=6 and O2 + Donor 2; n=6, Donor 3; n=6). **(E)** Fulton's index quantifying right ventricular hypertrophy (RA untreated; n=18, O2 + PBS; n=14, Donor 1; n=6 and O2 + Donor 2; n=6, Donor 3; n=6). Individual rats are represented by each dot. Values are represented as the mean ± STD. Significant results calculated by ordinary one-way ANOVA with Tukey's multiple comparison post hoc test. *: $p \leq 0.05$, **: $p \leq 0.01$, ***: $p \leq 0.001$, and ****: $p \leq 0.0001$.

4.2 Treatment with EVs isolated by TFF and dUC from Donor 1 did not improve lung function, PH or RVH in a hyperoxia-induced rat BPD model.

This experiment aimed to compare the efficacy of dUC-derived UC-MSC EVs to TFF-derived UC-MSC EVs in the rat BPD model and identify the optimal method for generating UC-MSC EVs. Donor 1 was chosen for this experiment due to its previous therapeutic effect on lung function.

800mL of CdM was collected from Donor 1 UC-MSCs at passage number (PN) 3 up to PN5. The CdM was collected from a total of 58 million cells. Half of the media was used to generate EVs using dUC and the other half was used to generate the media using TFF. EVs were characterized using the Bradford assay for protein quantification and nanoparticle tracking analysis for particle concentration and distribution. Results showed that TFF yields approximately five times more particles and protein when compared to dUC, however, dUC yields to EVs with a lower median size **(Table 2)**.

Table 2. Summary table of cell source, cell passage, nanoparticle tracking analysis, median particle size, protein concentration and cell equivalent value of dUC- and TFF-derived EVs. TFF yields around five times more particles and protein when compared to dUC. However, dUC yields to EVs with a lower median size.

Isolation technique	*Ultracentrifugation*	*TFF (300kDa)*
Cell source	**UC-MSCs**	**UC-MSCs**
Cell passage	**3-5**	**3-5**
NTA (particles/mL)	**5×10^{10}**	**22.4×10^{10}**
NTA (particles/million cells)	**7.01×10^{8}**	**3.16×10^{9}**
Median particle size (nm)	**136.8**	**151**
Protein (µg/µl)	**0.170**	**0.856**
Cell equivalent value	**28.436×10^{6}**	**29×10^{6}**

dUC-derived EVs and TFF-derived EVs were tested for their therapeutic potential in the same hyperoxia-induced lung injury model in neonatal rats as described previously **(Figure 9A)**. EVs were administered during the saccular stage of lung development in neonatal rats at P4, corresponding to the stage at which preterm infants who develop BPD are born **(Figure 9A)**. No significant differences in survival were observed in all groups **(Figure 9B)**. Pressure-volume (PV)-loop FlexiVent measurement was used to assess lung function **(Figure 9C)**. A significant decrease in delivery volume at 30 cmH_2O (peak pressure) was observed in the lung injury PBS group, indicating a strong disease model, however, dUC-derived EVs and TFF-derived EVs did not improve lung function **(Figure 9D)**. Lung injury significantly decreased PAAT/PAET ratio and increased RVH, however, dUC-derived EVs and TFF-derived EVs were unable to restore PAAT/PAET or RVH **(Figure 9E, F)**.

In summary, this experiment shows that although Donor 1 UC-MSCs improved lung function in the previous experiment, their EVs derived through dUC and TFF did not.

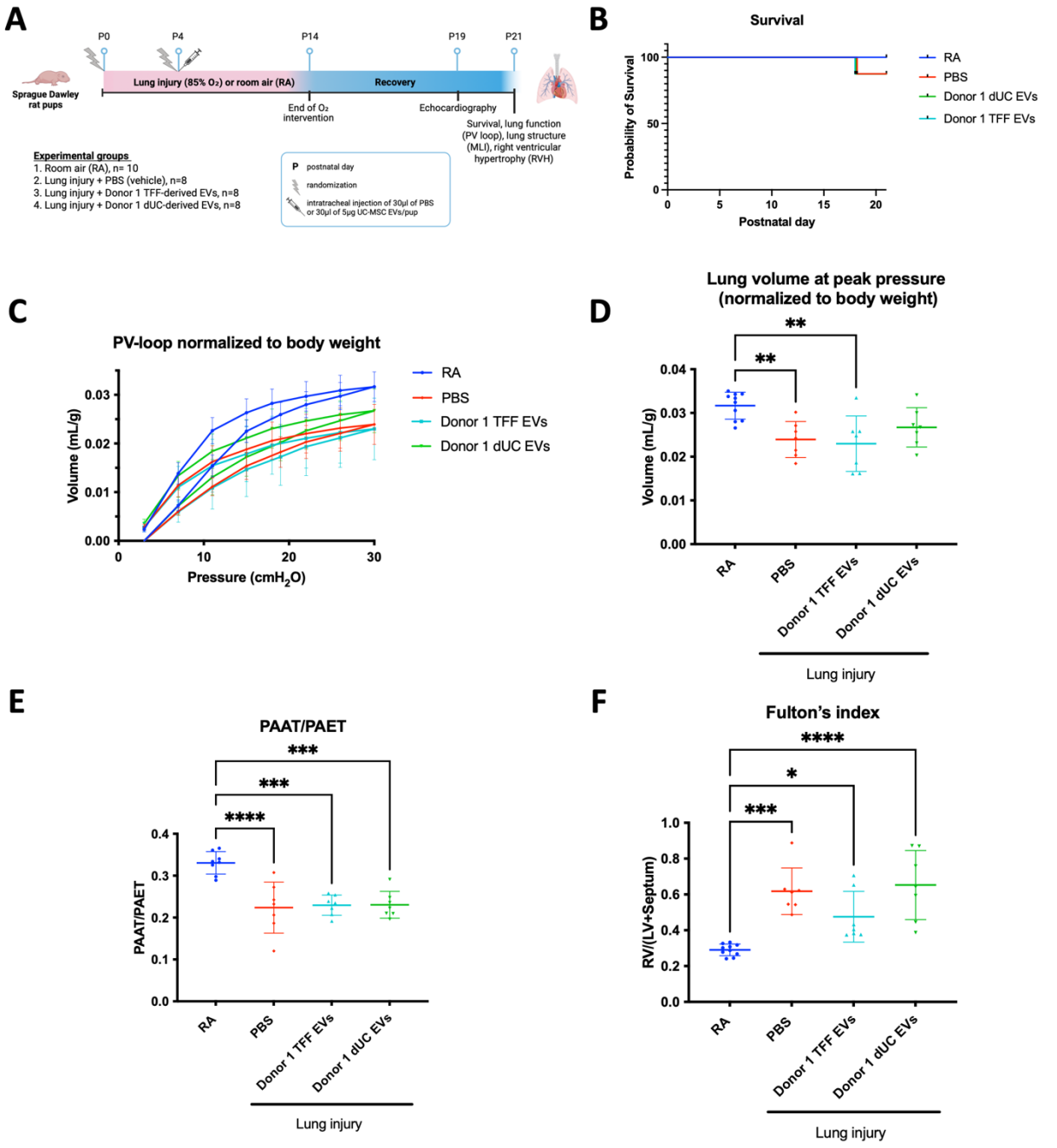

Figure 9. Treatment with EVs isolated by TFF and dUC from Donor 1 did not improve lung function, PH or RVH in a hyperoxia-induced rat BPD model. A) Schematic representation of the hyperoxia-induced lung injury model in neonatal rats as well as timelines for injections and endpoints. **(B)** Survival rate (%) on postnatal day 21. **(C)** Body weight-adjusted pressure volume

(PV)-loops curves where each loop represents the mean lung volume of all pups within one group at each pressure point (RA untreated; n=10, O2 + PBS; n=7, O2 + TFF-derived EVs; n=7 and O2 + dUC-derived EVs; n=7). **(D)** Body weight-adjusted inspiratory capacity (mL/g). **(E)** PAAT/PAET ratio were measured on echocardiography images (RA untreated; n=10, O2 + PBS; n=7, O2 + TFF-derived EVs; n=7 and O2 + dUC-derived EVs; n=7). **(F)** Fulton's index quantifying right ventricular hypertrophy (RA untreated; n=10, O2 + PBS; n=7, O2 + TFF-derived EVs; n=7 and O2 + dUC-derived EVs; n=7). Individual rats represented by each dot. Values are represented as the mean ± STD. Significant results calculated by ordinary one-way ANOVA with Tukey's multiple comparison post hoc test. *: $p \leq 0.05$, **: $p \leq 0.01$, ***: $p \leq 0.001$, and ****: $p \leq 0.0001$.

4.4 iMSCs from a single donor improved RVH and PAAT/PAET whereas UC-MSCs from different donors provided various levels of therapeutic effects in a hyperoxia-induced rat BPD model.

Our lab has previously shown that UC-MSCs isolated from different donors can have different transcriptomic profiles that could dictate their therapeutic efficacy (101). For example, UC-MSCs with a progenitor-like transcriptome had a therapeutic effect on lung structure, lung function, PAAT/PAET and RVH whereas UC-MSCs that had a fibroblast-like transcriptome did not. However, in clinical settings, it might be challenging to analyze the transcriptome of all UC-MSC donors. Therefore, we became interested in exploring iMSCs as a new potential therapeutic candidate for BPD. iMSCs became a major interest for us due to their ability to limit donor-to-donor variability because only a single donor would be used. We decided to compare the effect of iMSCs to UC-MSCs from additional donors. Thus, each experiment has an iMSC group and a UC-MSC group tested side-by-side.

First, we analyzed the cell surface markers panel proposed by ISCT **(Supplementary Figure 1)**. UC-MSCs were used as a positive control and ECFCs were used as a negative control for CD90. DAPI was included to measure viability. iMSCs were found to express the following:

CD73 (96.3%), CD90 (61.4%), CD105 (74.5%), CD34-CD11b-CD19-CD45-HLA-DR (2.62%). UC-MSCs expressed the following: CD73 (97.8%), CD90 (98.6%), CD105 (91.6%), CD34-CD11b-CD19-CD45-HLA-DR (0.75%). Finaly, ECFCs expressed the following: CD73 (79.8%), CD90 (0.021%), CD105 (99.8%), CD34-CD11b-CD19-CD45-HLA-DR (4.81%).

Next, we conducted an *in vivo* experiment. We collaborated with the Cell Manufacturing Facility (CMF) to obtain well-characterized UC-MSCs from Donor 4, 5 and 6 **(Supplementary Figure 2)**. In this experiment, we injected Donor 4 UC-MSCs and iMSCs at P4 **(Figure 10A)**. Although not statistically significant, a substantial number of pups died in the Donor 5 group and PBS group (n=5 deaths/group) whereas only one pup died in the iMSC group **(Figure 10B)**. In addition, body weight analysis revealed that the lung injury groups had a significantly lower body weight than the RA group **(Supplementary Figure 3A)**. These results indicate that the disease model was severe. PV-loop FlexiVent measurement was used to assess lung function **(Figure 10C)**. Delivery volume at 30 cmH_2O (peak pressure) significantly decreased in the lung injury PBS group, indicating a strong disease model, however, Donor 4 UC-MSCs and iMSCs did not improve lung function **(Figure 10D)**. Lung injury significantly decreased PAAT/PAET and increased the RVH, however, Donor 4 UC-MSCs and iMSCs were unable to restore PAAT/PAET and only the iMSCs were able to reduce RVH **(Figure 10E,F)**. Neither Donor 4 UC-MSCs or iMSCs significantly improved lung structure (quantified by MLI) **(Figure 10G)**.

In summary, this experiment shows that iMSCs provided superior therapeutic effects on survival and RVH compared to Donor 4 UC-MSCs. This highlights the potential benefits of using iMSCs from a single donor to overcome inter-donor variability present in tissue-derived MSCs.

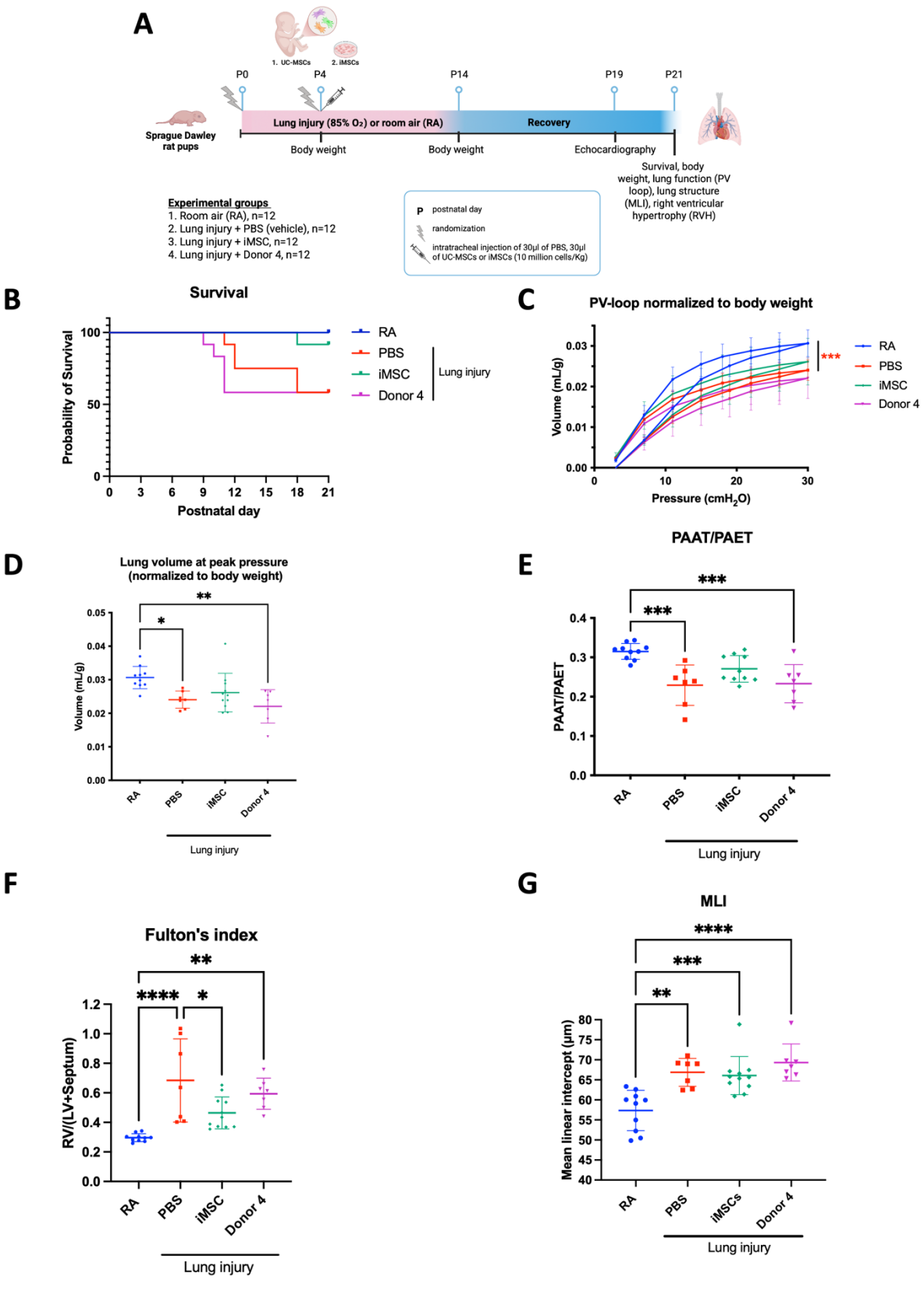
A
1. UC-MSCs
2. iMSCs
P0
P4
P14
P19
P21
Sprague Dawley rat pups
Lung injury (85% O2) or room air (RA)
Recovery
Body weight
Body weight
Echocardiography
Survival, body weight, lung function (PV loop), lung structure (MLI), right ventricular hypertrophy (RVH)
Experimental groups
1. Room air (RA), n=12
2. Lung injury + PBS (vehicle), n=12
3. Lung injury + iMSC, n=12
4. Lung injury + Donor 4, n=12
P postnatal day
randomization
intratracheal injection of 30µl of PBS, 30µl of UC-MSCs or iMSCs (10 million cells/Kg)
B
Survival
Probability of Survival
Postnatal day
RA
PBS
iMSC
Donor 4
Lung injury
C
PV-loop normalized to body weight
Volume (mL/g)
Pressure (cmH2O)
***
RA
PBS
iMSC
Donor 4
D
Lung volume at peak pressure (normalized to body weight)
Volume (mL/g)
RA
PBS
iMSC
Donor 4
Lung injury
E
PAAT/PAET
PAAT/PAET
Lung injury
F
Fulton's index
RV/(LV+Septum)
Lung injury
G
MLI
Mean linear intercept (µm)
RA
PBS
iMSCs
Donor 4
Lung injury

Figure 10. Treatment with iMSCs improve RVH in a hyperoxia-induced rat BPD model whereas UC-MSCs isolated from Donor 4 did not. (A) Schematic representation of the hyperoxia-induced lung injury model in neonatal rats as well as timelines for injections and endpoints. **(B)** Survival rate (%) on postnatal day 21. **(C)** Body weight-adjusted pressure volume (PV)-loops curves where each loop represents the mean lung volume of all pups within one group at each pressure point (RA untreated; n=10, O2 + PBS; n=7, O2 + iMSCs; n=11, O2 + Donor 4; n=7). **(D)** Body weight-adjusted inspiratory capacity (mL/g). **(E)** PAAT/PAET ratio where PAAT is pulmonary arterial acceleration time and PAET is pulmonary arterial ejection time. PAAT and PAET were measured on echocardiography images (RA untreated; n=10, O2 + PBS; n=7, O2 + iMSCs; n=10 (1 difficult to measure), O2 + Donor 4; n=7). **(F)** Fulton's index quantifying right ventricular hypertrophy (RA untreated; n=10, O2 + PBS; n=7, O2 + iMSCs; n=11, O2 + Donor 4; n=7). **(G)** Mean linear intercept (MLI) (RA untreated; n=10, O2 + PBS; n=7, O2 + iMSCs; n=11, O2 + Donor 4; n=7). Individual rats represented by each dot. Values are represented as the mean ± STD. Significant results calculated by ordinary one-way ANOVA with Tukey's multiple comparison post hoc test. *: $p \leq 0.05$, **: $p \leq 0.01$, ***: $p \leq 0.001$, and ****: $p \leq 0.0001$.

We repeated the previous experiment with a different UC-MSC donor (Donor 5) to assess the reproducibility of the positive effects provided by iMSCs on survival and RVH. We injected Donor 5 UC-MSCs and iMSCs at P4 **(Figure 11A)**. Due to technical difficulties with expanding the iMSCs in culture this time, we were only able to inject 7 pups with iMSCs and included more pups in the PBS and Donor 5 groups. No significant differences between survival were observed in all groups **(Figure 11B)**. Unlike experiment 4, body weight analysis did not reveal that all the lung injury groups had a significantly lower body weight than the RA group, suggesting a less severe model **(Supplementary Figure 3B)**. PV-loop FlexiVent measurement was used to assess lung function **(Figure 11C)**. Delivery volume at 30 cmH_2O (peak pressure) significantly decreased in the lung injury PBS group, indicating a strong disease model, however, Donor 5 UC-MSCs and iMSCs did not improve lung function **(Figure 11D)**. Lung injury significantly decreased PAAT/PAET and increased the RVH, however, Donor 5 UC-MSCs and iMSCs were unable to restore PAAT/PAET or RVH **(Figure 11E,F)**. Neither Donor 5 UC-MSCs or iMSCs significantly improved lung structure (MLI) **(Figure 11G)**.

In summary, this experiment shows that the model is less severe than the previous experiment and that the iMSCs and Donor 5 UC-MSCs did not provide significant therapeutic effects.

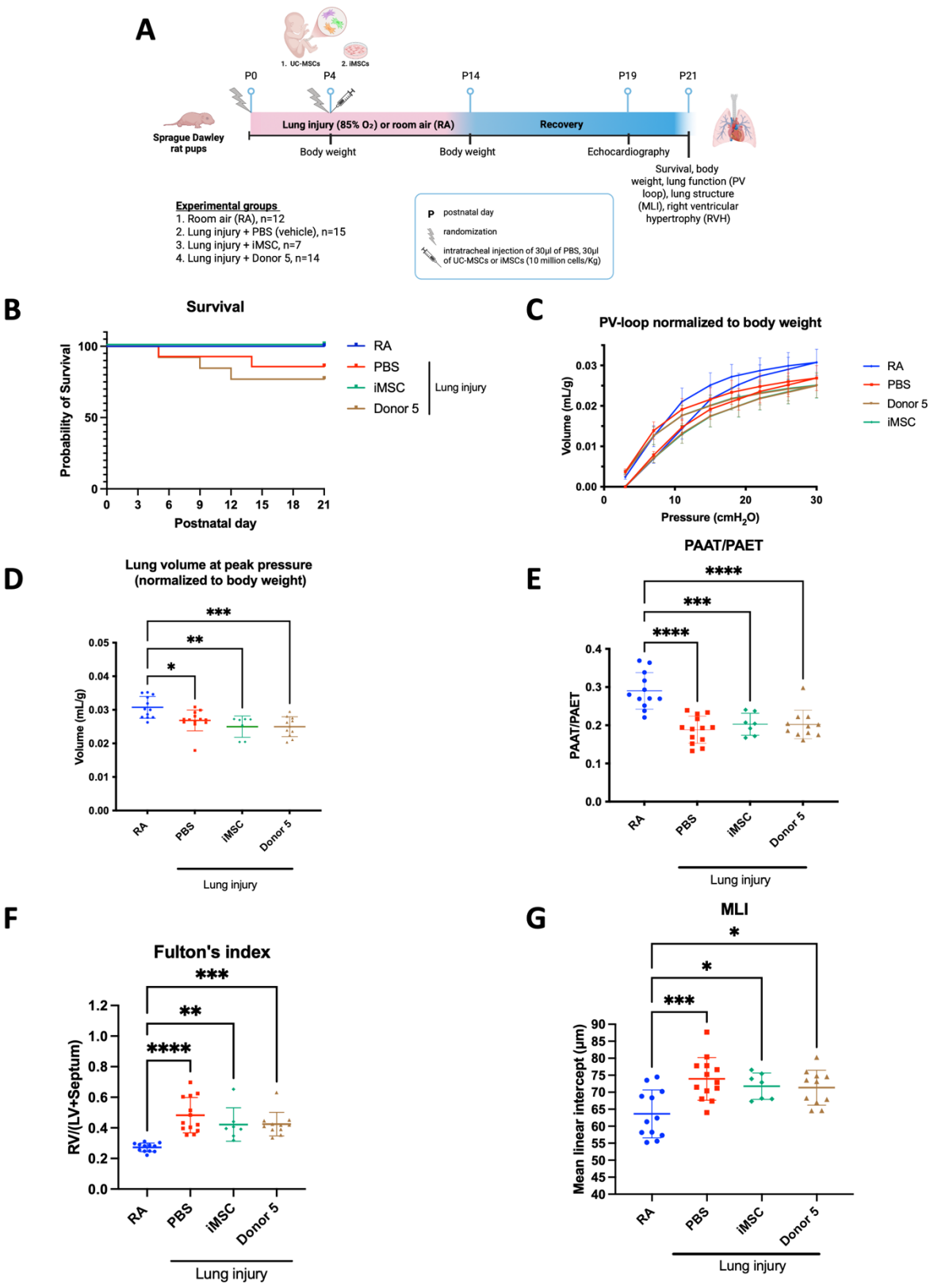
A
1. UC-MSCs
2. iMSCs
P0
P4
P14
P19
P21
Sprague Dawley rat pups
Lung injury (85% O2) or room air (RA)
Recovery
Body weight
Body weight
Echocardiography
Survival, body weight, lung function (PV loop), lung structure (MLI), right ventricular hypertrophy (RVH)
Experimental groups
1. Room air (RA), n=12
2. Lung injury + PBS (vehicle), n=15
3. Lung injury + iMSC, n=7
4. Lung injury + Donor 5, n=14
P postnatal day
randomization
intratracheal injection of 30µl of PBS, 30µl of UC-MSCs or iMSCs (10 million cells/Kg)
B
Survival
Probability of Survival
Postnatal day
RA
PBS
iMSC
Donor 5
Lung injury
C
PV-loop normalized to body weight
Volume (mL/g)
Pressure (cmH2O)
RA
PBS
Donor 5
iMSC
D
Lung volume at peak pressure (normalized to body weight)
Volume (mL/g)
RA
PBS
iMSC
Donor 5
Lung injury
E
PAAT/PAET
PAAT/PAET
RA
PBS
iMSC
Donor 5
Lung injury
F
Fulton's index
RV/(LV+Septum)
RA
PBS
iMSC
Donor 5
Lung injury
G
MLI
Mean linear intercept (µm)
RA
PBS
iMSC
Donor 5
Lung injury

Figure 11. Treatment with iMSCs and UC-MSCs isolated from Donor 5 did not provide significant therapeutic effects in a hyperoxia-induced rat BPD model. (A) Schematic representation of the hyperoxia-induced lung injury model in neonatal rats as well as timelines for injections and endpoints. **(B)** Survival rate (%) on postnatal day 21. **(C)** Body weight-adjusted pressure volume (PV)-loops curves where each loop represents the mean lung volume of all pups within one group at each pressure point (RA untreated; n=12, O2 + PBS; n=13, O2 + iMSCs; n=7, O2 + Donor 5; n=11). **(D)** Body weight-adjusted inspiratory capacity (mL/g). **(E)** PAAT/PAET ratio where PAAT is pulmonary arterial acceleration time and PAET is pulmonary arterial ejection time. PAAT and PAET were measured on echocardiography images RA untreated; n=12, O2 + PBS; n=13, O2 + iMSCs; n=7, O2 + Donor 5; n=11. **(F)** Fulton's index quantifying right ventricular hypertrophy (RA untreated; n=12, O2 + PBS; n=13, O2 + iMSCs; n=7, O2 + Donor 5; n=11). **(G)** MLI (RA untreated; n=12, O2 + PBS; n=13, O2 + iMSCs; n=7, O2 + Donor 5; n=11). (Individual rats represented by each dot. Values are represented as the mean ± STD. Significant results calculated by ordinary one-way ANOVA with Tukey's multiple comparison post hoc test. *: $p \leq 0.05$, **: $p \leq 0.01$, ***: $p \leq 0.001$, and ****: $p \leq 0.0001$.

Although the results from the last experiment did not match the results obtained from the first iMSC experiment, we were still interested in further testing those iMSCs. In this experiment, we injected UC-MSCs from Donor 6 and iMSCs at P4 **(Figure 12A)**. We were able to overcome the technical difficulties with expanding the iMSCs for this experiment. No significant differences between survival were observed in all groups **(Figure 12B)**. Body weight analysis did not reveal any major differences in body weight across groups **(Supplementary Figure 3C)**. PV-loop FlexiVent measurement was used to assess lung function **(Figure 12C)**. Delivery volume at 30 cmH_2O (peak pressure) significantly decreased in the lung injury PBS group, indicating a strong disease model, however, Donor 6 UC-MSCs and iMSCs did not improve lung function **(Figure 12D)**. Lung injury significantly decreased PAAT/PAET and increased RVH, however, Donor 6 UC-MSCs and iMSCs were unable to restore PAAT/PAET or RVH **(Figure 12E,F)**.

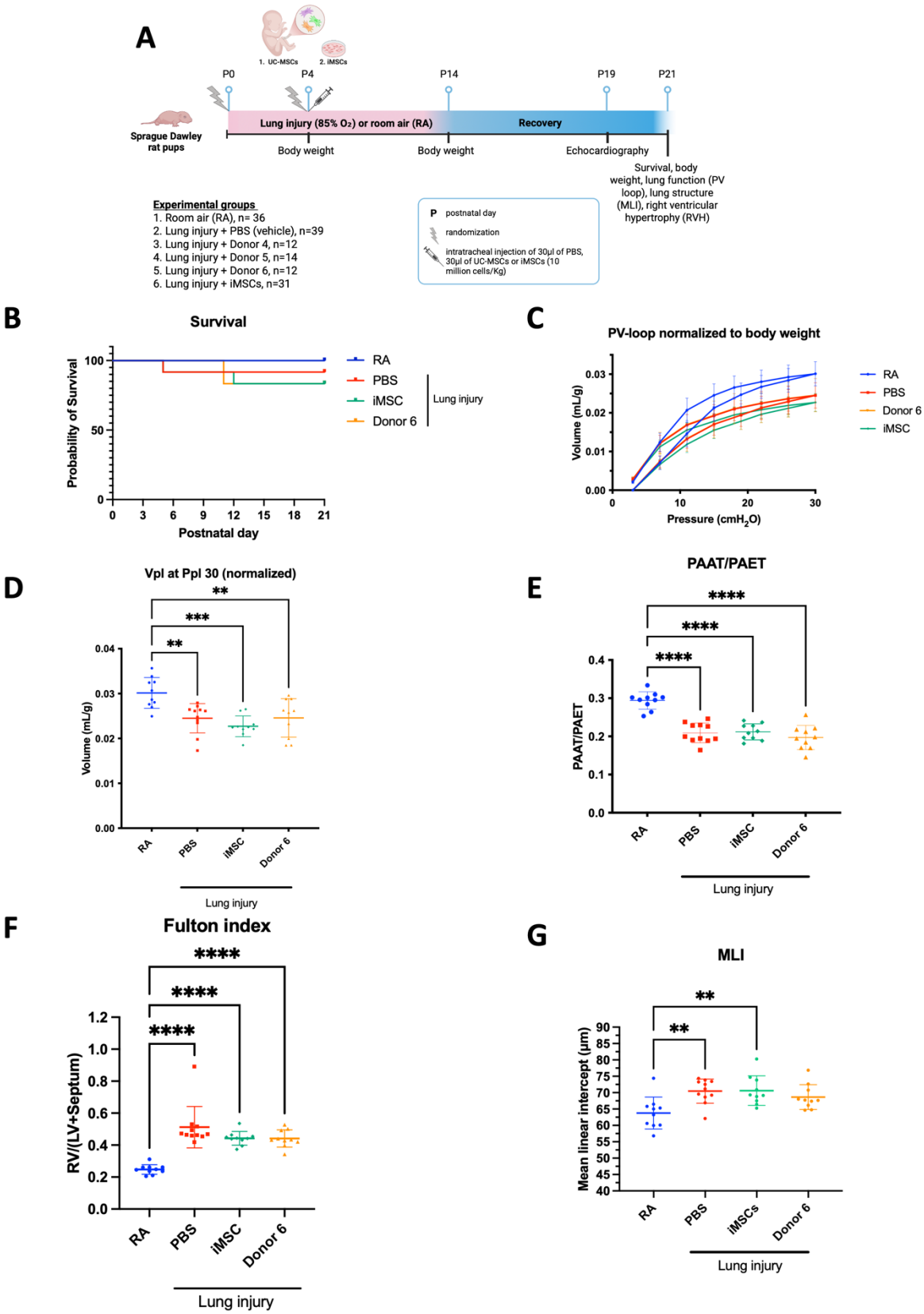
A
1. UC-MSCs
2. iMSCs
P0
P4
P14
P19
P21
Sprague Dawley rat pups
Lung injury (85% O2) or room air (RA)
Recovery
Body weight
Body weight
Echocardiography
Survival, body weight, lung function (PV loop), lung structure (MLI), right ventricular hypertrophy (RVH)
Experimental groups
1. Room air (RA), n= 36
2. Lung injury + PBS (vehicle), n=39
3. Lung injury + Donor 4, n=12
4. Lung injury + Donor 5, n=14
5. Lung injury + Donor 6, n=12
6. Lung injury + iMSCs, n=31
P postnatal day
randomization
intratracheal injection of 30µl of PBS, 30µl of UC-MSCs or iMSCs (10 million cells/Kg)
B
Survival
Probability of Survival
Postnatal day
RA
PBS
iMSC
Donor 6
Lung injury
C
PV-loop normalized to body weight
Volume (mL/g)
Pressure (cmH2O)
RA
PBS
Donor 6
iMSC
D
Vpl at Ppl 30 (normalized)
Volume (mL/g)
RA
PBS
iMSC
Donor 6
Lung injury
E
PAAT/PAET
PAAT/PAET
RA
PBS
iMSC
Donor 6
Lung injury
F
Fulton index
RV/(LV+Septum)
RA
PBS
iMSC
Donor 6
Lung injury
G
MLI
Mean linear intercept (µm)
RA
PBS
iMSCs
Donor 6
Lung injury

Figure 12. Treatment with iMSCs and UC-MSCs isolated from Donor 6 did not provide significant therapeutic effects in a hyperoxia-induced rat BPD model. A) Schematic representation of the hyperoxia-induced lung injury model in neonatal rats as well as timelines for injections and endpoints. **(B)** Survival rate (%) on postnatal day 21. **(C)** Body weight-adjusted pressure volume (PV)-loops curves where each loop represents the mean lung volume of all pups within one group at each pressure point (RA untreated; n=10, O2 + PBS; n=11, O2 + iMSCs; n=10, O2 + Donor 6; n=10). **(D)** Body weight-adjusted inspiratory capacity (mL/g). **(E)** PAAT/PAET ratio where PAAT is pulmonary arterial acceleration time and PAET is pulmonary arterial ejection time. PAAT and PAET were measured on echocardiography images (RA untreated; n=10, O2 + PBS; n=11, O2 + iMSCs; n=10, O2 + Donor 6; n=10). **(F)** Fulton's index quantifying right ventricular hypertrophy (RA untreated; n=10, O2 + PBS; n=11, O2 + iMSCs; n=10, O2 + Donor 6; n=10). **(G)** MLI (RA untreated; n=10, O2 + PBS; n=11, O2 + iMSCs; n=10, O2 + Donor 6; n=10). Individual rats represented by each dot. Values are represented as the mean ± STD. Significant results calculated by ordinary one-way ANOVA with Tukey's multiple comparison post hoc test. *: $p \leq 0.05$, **: $p \leq 0.01$, ***: $p \leq 0.001$, and ****: $p \leq 0.0001$.

Here, we provide grouped and sub-group analysis of the combined data from the three iMSC experiments. The consort chart outlines the flow of our experimental design and highlights key interventions and assessments as well as excluded animals and death outcomes **(Figure 13**).

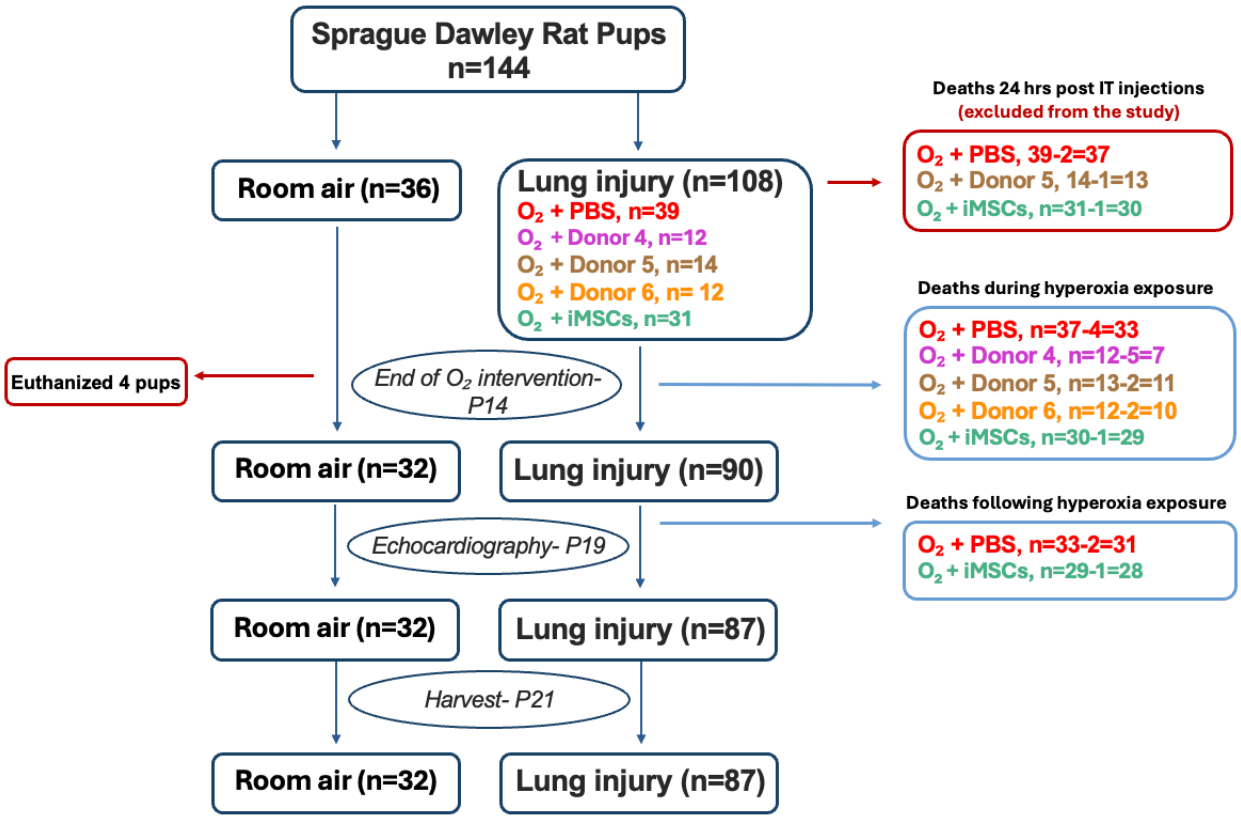

Figure 13. CONSORT flowchart for experiments 4, 5 and 6 combined. 144 SD rat pups were exposed to either room air (RA) or lung injury (O_2). Within the lung injury groups, the rat pups either received PBS, Donor 4 UC-MSCs, Donor 5 UC-MSCs, Donor 6 UC-MSCs or iMSCs. Animals within the red boxes have been excluded from the study. Postnatal day (P) 14 marks the end of O_2 intervention. At P19, echocardiography assessment is performed in all animals to measure PAAT/PAET. At P21, all the animals are harvested for lung function, lung structure and RVH analysis.

Grouped analysis demonstrate that after testing UC-MSC Donor 4, 5 and 6 and iMSCs in the same rat BPD model, iMSCs provide favorable outcomes on survival and RVH whereas Donor 5 UC-MSCs provide favorable outcomes on RVH and Donor 4 and 6 UC-MSCs provide no therapeutic effects **(Figure 14A, B, F)**. However, none of the treatments provided a significant effect on lung function and PAAT/PAET **(Figure 14C,D,E)**. Similarly, grouped analysis show that iMSCs provide favorable outcomes on survival and RVH whereas UC-MSCs from Donor 1, 2 and 3 did not **(Supplementary Figure 6B)**. However, UC-MSCs from Donor 1 were superior in

restoring lung function compared to iMSCs and UC-MSCs from Donor 2 and 3 **(Supplementary Figure 6A)**.

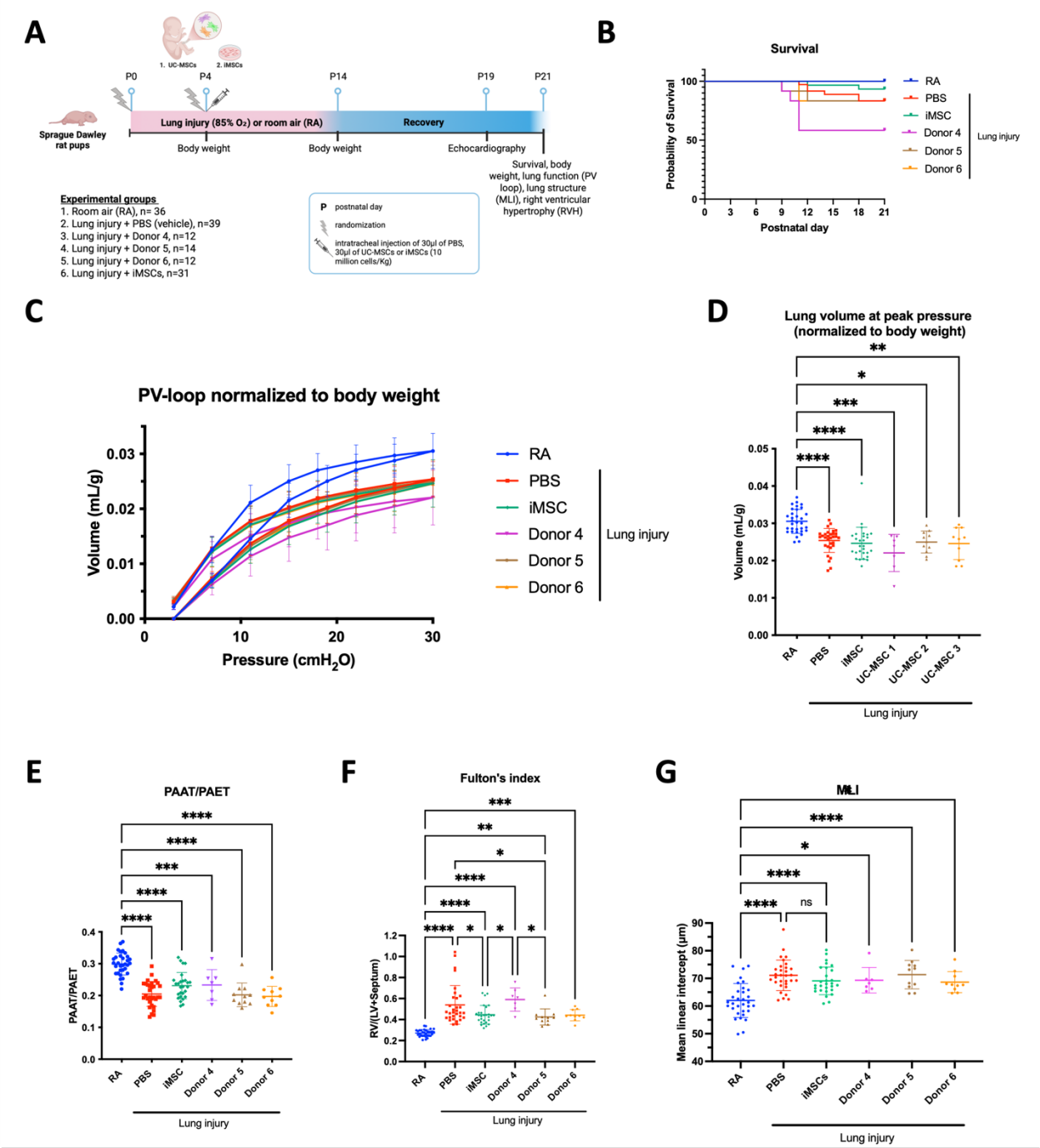

Figure 14. Grouped analysis of the data generated from all 3 iMSC experiments suggest that iMSCs and Donor 5 UC-MSCs improve PH in in a hyperoxia-induced rat BPD model. (A) Schematic representation of the hyperoxia-induced lung injury model in neonatal rats as well as

timelines for injections and endpoints. **(B)** Survival rate (%) on postnatal day 21 (RA untreated; n=32, O2 + PBS; n=31, O2 + iMSCs; n=28, O2 + Donor 4; n=7, O2 + Donor 5; n=11, O2 + Donor 6; n=10). **(C)** Body weight-adjusted pressure volume (PV)-loops curves where each loop represents the mean lung volume of all pups within one group at each pressure point (RA untreated; n=32, O2 + PBS; n=31, O2 + iMSCs; n=28, O2 + Donor 4; n=7, O2 + Donor 5; n=11, O2 + Donor 6; n=10). **(D)** Body weight-adjusted inspiratory capacity (mL/g). Individual rats represented by each dot (RA untreated; n=32, O2 + PBS; n=31, O2 + iMSCs; n=28, O2 + Donor 4; n=7, O2 + Donor 5; n=11, O2 + Donor 6; n=10). **(E)** PAAT/PAET ratio where PAAT is pulmonary arterial acceleration time and PAET is pulmonary arterial ejection time. PAAT and PAET were measured on echocardiography images (RA untreated; n=32, O2 + PBS; n=31, O2 + iMSCs; n=27 (1 difficult to measure), O2 + Donor 4; n=7, O2 + Donor 5; n=11, O2 + Donor 6; n=10). **(F)** Fulton's index quantifying right ventricular hypertrophy (right ventricle weight/left ventricle + septum weight) (RA untreated; n=32, O2 + PBS; n=31, O2 + iMSCs; n=28, O2 + Donor 4; n=7, O2 + Donor 5; n=11, O2 + Donor 6; n=10). **(G)** MLI (RA untreated; n=32, O2 + PBS; n=31, O2 + iMSCs; n=28, O2 + Donor 4; n=7, O2 + Donor 5; n=11, O2 + Donor 6; n=10). Individual rats represented by each dot. Values are represented as the mean ± STD. Significant results calculated by ordinary one-way ANOVA with Tukey's multiple comparison post hoc test. *: $p \leq 0.05$, **: $p \leq 0.01$, ***: $p \leq 0.001$, and ****: $p \leq 0.0001$.

Similarly, sub-group analysis of RVH demonstrate that the iMSCs and Donor 5 UC-MSCs provide a significant effect on RVH whereas Donor 4 and 6 UC-MSCs did not **(Figure 15)**.

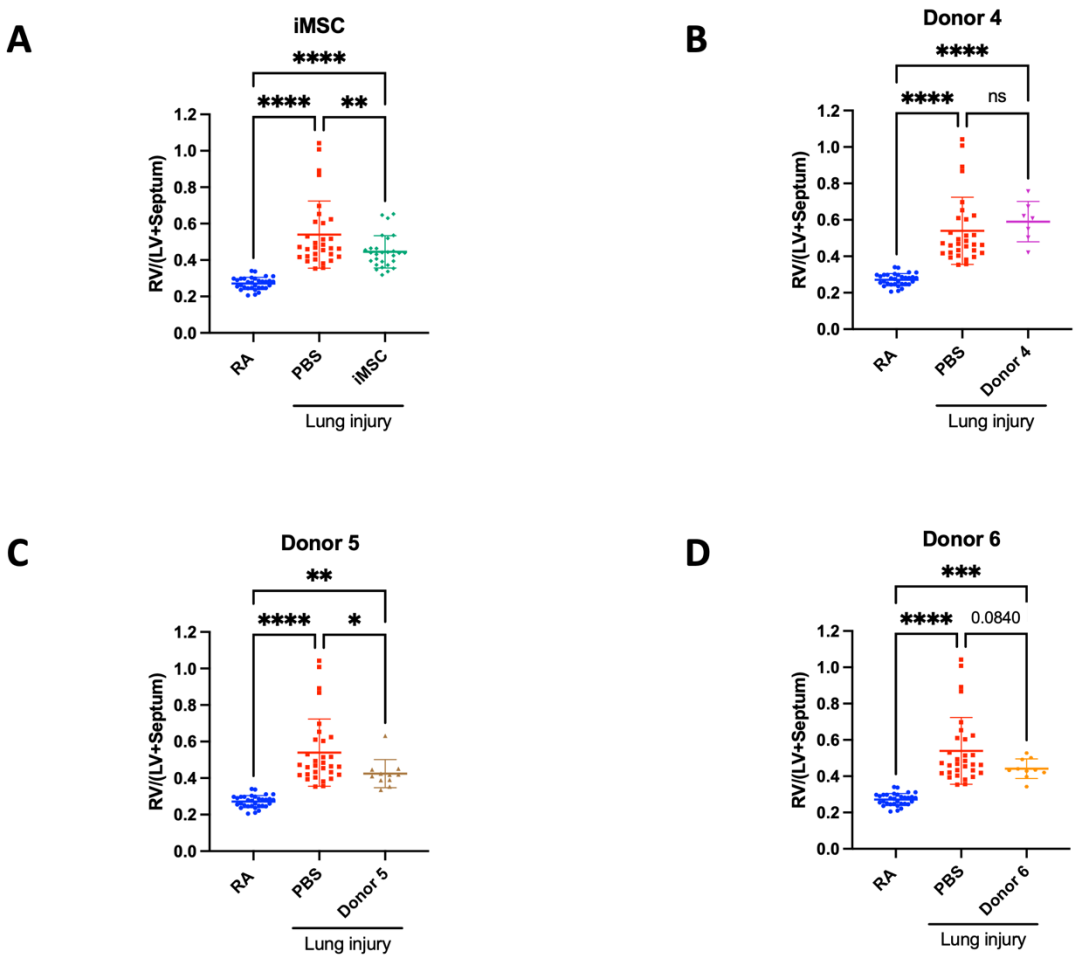

Figure 15. Right ventricular hypertrophy sub-group analysis. (A) Fulton's index quantifying right ventricular hypertrophy (right ventricle weight/left ventricle + septum weight) (RA untreated; n=32, O2 + PBS; n=31, O2 + iMSCs; n=28). **(B)** Fulton's index quantifying right ventricular hypertrophy (RA untreated; n=32, O2 + PBS; n=31, Donor 4 UC-MSCs; n=7). **(C)** Fulton's index quantifying right ventricular hypertrophy (RA untreated; n=32, O2 + PBS; n=31, O2 + Donor 5 UC-MSCs; n=11). **(D)** Fulton's index quantifying right ventricular hypertrophy (RA untreated; n=32, O2 + PBS; n=31, O2 + Donor 6 UC-MSCs; n=10). Individual rats represented by each dot. Values are represented as the mean ± STD. Significant results calculated by ordinary one-way ANOVA with Tukey's multiple comparison post hoc test. *: $p \leq 0.05$, **: $p \leq 0.01$, ***: $p \leq 0.001$, and ****: $p \leq 0.0001$.

Furthermore, sub-group analysis of PAAT/PAET demonstrate that iMSCs significantly improve PAAT/PAET whereas the UC-MSCs did not **(Figure 16)**.

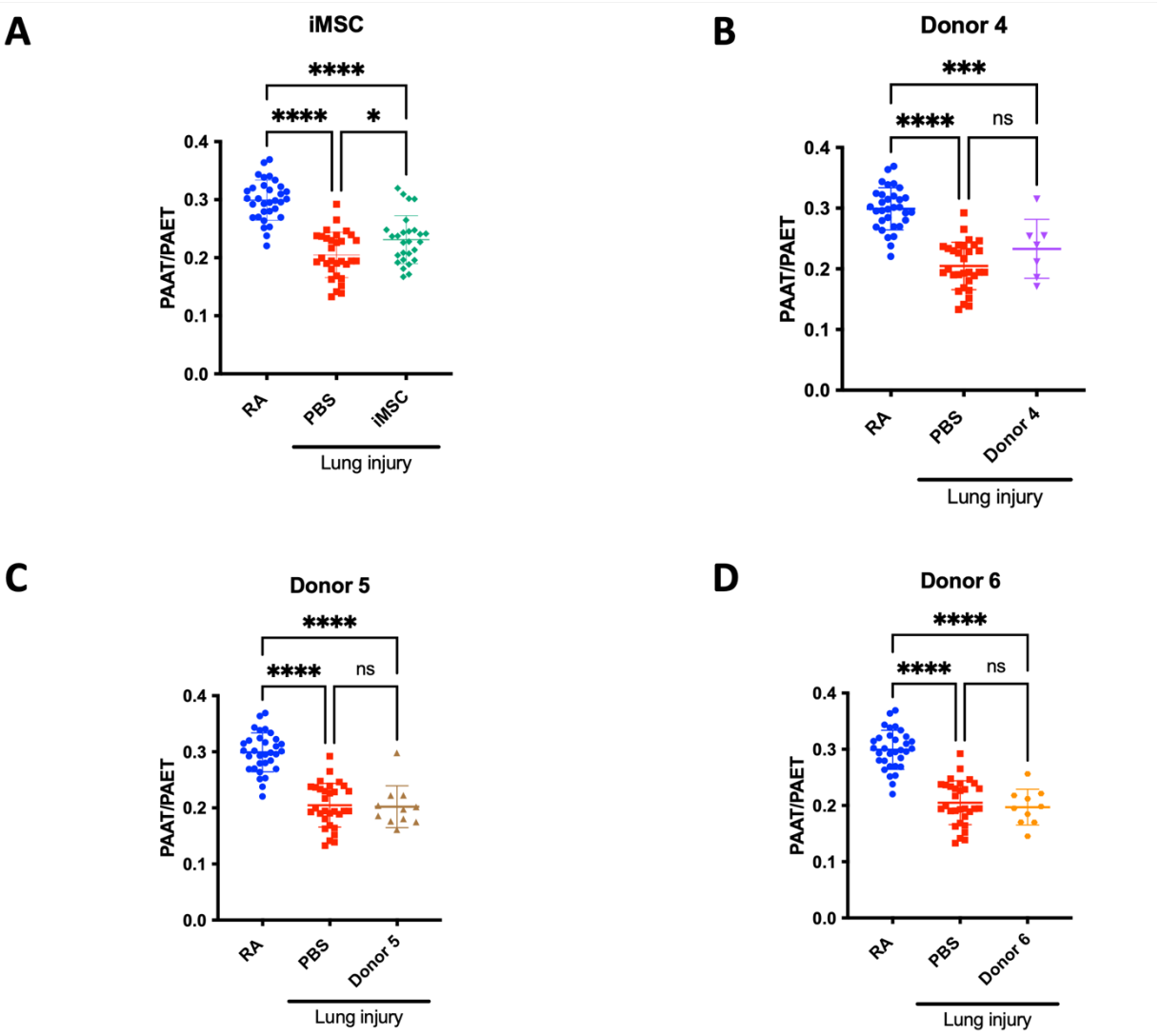

Figure 16. Echocardiography sub-group analysis. (A) PAAT/PAET ratio were measured on echocardiography images (RA untreated; n=32, O2 + PBS; n=31, O2 + iMSCs; n=27 (1 difficult to measure)). **(B)** PAAT/PAET ratio were measured on echocardiography images (RA untreated; n=32, O2 + PBS; n=31, Donor 4 UC-MSCs; n=7). **(C)** PAAT/PAET ratio were measured on echocardiography images (RA untreated; n=32, O2 + PBS; n=31, O2 + Donor 5 UC-MSCs; n=11). **(D)** PAAT/PAET ratio were measured on echocardiography images (RA untreated; n=32, O2 + PBS; n=31, O2 + Donor 6 UC-MSCs; n=10). Individual rats represented by each dot. Values are represented as the mean ± STD. Significant results calculated by ordinary one-way ANOVA with Tukey's multiple comparison post hoc test. *: $p \leq 0.05$, **: $p \leq 0.01$, ***: $p \leq 0.001$, and ****: $p \leq 0.0001$.

Given that the iMSCs outperformed most UC-MSCs in improving PAAT/PAET, RVH and survival, we were interested in trying to find a possible mechanism of action of iMSCs. One such mechanism is the expression of indoleamine 2,3 deoxygenase (IDO) as it is described as an essential factor for the immunomodulatory function of MSCs (102). We exposed UC-MSCs from Donor 4, 5, 6 and the iMSCs to interferon-gamma (IFN-γ) for 24 hours then harvested the cells, extracted their RNA and performed RT-qPCR to determine IDO expression levels. Our results showed that although all the cells met the minimum criteria for clinical trials, which is a 5-fold increase in IDO expression following exposure to IFN-γ, the iMSCs had the least increase in IDO expression **(Supplementary Figure 5)**. Since this assay was done only once, it needs to be repeated before determining whether it could accurately predict the therapeutic effect of MSCs *in vivo*.

5. Discussion

In this body of work, we have demonstrated that: (1) UC-MSCs indeed possess inter-donor variability which causes them to provide different levels of therapeutic efficacy in a neonatal rat lung injury model, (2) TFF is a more scalable method for UC-MSC EV isolation which generates five times more particles and protein than dUC, (3) iPSCs could potentially offer a more uniform source of iMSCs with a high therapeutic potential highlighted by their ability to significantly improve RVH, PAAT/PAET and survival in some experiments and (4) MSC potency assays using IDO qPCR do not accurately predict MSC therapeutic effects *in vivo.*

Although advancements in perinatal care have contributed to higher survival rates of premature infants, the incidence of BPD remains constant in extremely preterm infants with 75% of those born between 22-24 weeks of GA developing BPD (24,103,104). Mechanical ventilation and intubation are used to treat critically ill neonates in the clinic to facilitate gas exchange, oxygenation and carbon dioxide removal (105). However, these lifesaving interventions also expose neonates to prolonged excessive oxygen levels, leading to high levels of inflammation and lung injury (106). Oxygen-induced inflammation may lead to the onset of chronic complications such as asthma, emphysema, reduced exercise capacity and PH (107–110). Despite being first reported in 1967, there are still no effective treatments for BPD (111).

MSCs present a promising avenue to treat BPD due to their great regenerative and immunomodulatory potential. However, while MSCs have been tested in more than 1,000 clinical trials for a range of diseases, only three Phase III clinical trials have been completed and only one MSC product (OSSM-001) received FDA approval (62,63). In Canada, only one MSC product (Prochymal) received Health Canada approval for treating pediatric patients with GvHD (112).

The heterogeneity of MSC populations could be a possible explanation for inconsistent results in the clinic (68). Therefore, standardizing MSC populations is an important consideration in clinical applications.

Our lab has attempted to find a subpopulation of MSCs that has superior therapeutic efficacy. We showed that UC-MSCs expressing high levels of human leukocyte antigen (HLA)-A, -B, and -C show reduced therapeutic effect in a hyperoxia-induced lung injury rat model (113). Subsequent experiments in our lab confirmed that UC-MSCs expressing high HLA-A,B,C were non-therapeutic on lung function and lung structure whereas UC-MSC expressing low HLA-A,B,C did not provide any effects either **(Supplementary Figure 4)**. Therefore, further research is required to enhance the efficacy of MSCs, understand their mechanism of action and identify a method to assess their therapeutic outcomes.

The first experiment highlights the inter-donor variability of UC-MSCs where Donor 1 improved lung function and Donor 2 and 3 did not. Multiple studies have investigated the heterogeneity of UC-MSCs using single-cell RNA sequencing (scRNA-seq) (114–121). Studies compared the transcriptomes of MSCs 1) isolated from different tissues (116,118,120,121), 2) exposed to different stimulations (IFNγ and TNFα), 3) at different PNs (117) and 4) that are primary versus cultured (114). However, most of these studies did not correlate MSC heterogeneity with their functions.

iMSCs represent a possible avenue for eliminating inter-donor variability because manufacturing iMSCs requires only a single donor. The manufacturing process has been described to consist of three main stages: 1) banking iPSCs, 2) expanding iPSCs and differentiating them to iMSCs and 3) expanding iMSCs to form a final clinical product. A single iPSC line has been estimated to produce 90,000 vials each containing 1 million iPSCs. A single vial of 1 million iPSCs

can generate 3.2×10^{10} iMSCs on average, whereas the entire iPSC bank can generate 2.9×10^{15} iMSCs. This could provide 29 million clinical doses each containing 1×10^{8} iMSCs (94). Given this ability of generating a large amount of iMSCs from a single donor, this technology will help eliminate inter-donor variability as one donor will be sufficient to support several clinical trials.

We hypothesized that UC-MSC EVs could provide similar therapeutic benefits to their parent cells. However, this was refuted by our results which showed that TFF- and dUC-derived UC-MSC EVs did not significantly improve lung function or RVH. We believe that a possible reason why a significant effect was not observed following treatment with TFF- and dUC-derived MSC EVs is the fact that this process required culturing the UC-MSCs for a long period of time (~2 weeks) up to passage 5. Evidence suggests that long-term culture causes MSCs to lose their differentiation ability and undergo morphological changes (122). Additionally, at higher passages, MSCs have been shown to age due to reduced telomerase activity (123). Therefore, it is important to repeat this experiment using large-scale systems to produce and collect EVs such as the hollow-fiber bioreactor system (124). iPSCs can overcome this problem by ensuring an unlimited source of cells for MSC differentiation (125). Therefore, we decided to pivot this project towards investigating iMSCs. We were interested in testing the iMSCs side-by-side with UC-MSCs to investigate whether the iMSCs perform similarly or better than UC-MSCs. This was made possible by partnering with Pluristyx, a biotechnology company specialized in iPSC-based products who manufactured and provided us with iMSCs to conduct our studies.

As discussed earlier, the ISCT developed minimal criteria to identify MSCs: 1) adhere to plastic, 2) display specific cell surface markers identified by flow cytometry (CD73+, CD90+, CD105+, CD34-, CD45-, CD14/CD11b-, CD79α/CD19-, HLA-DR), and 3) differentiate into osteoblasts, adipocytes, and chondrocytes (99). Given that we had a limited stock of iMSCs, we

decided to prioritize testing their cell surface marker expression. We started by characterizing iMSCs using flow cytometry to find out whether they satisfy the ISCT criteria **(Supplementary Figure 1**). The ISCT criteria state that MSCs must express positive markers (CD90, CD105 and CD73) at levels of at least 95% while expressing negative markers (CD45, CD34, CD14 or CD11b, CD79alpha or CD19, and HLA-DR) at levels of at most 2%. While the UC-MSCs generally met those criteria, the iMSCs did not meet the criteria for CD90 and CD105. iMSCs also expressed CD34-CD11b-CD19-CD45-HLA-DR at 2.62%, exceeding the ISCT recommendations for negative markers. ECFCs served as a negative control for CD90 while highly expressing CD105, as expected.

Other studies also show that iMSCs do not strictly meet the ISCT criteria for cell surface markers (126–128). A study done by Lee, et al. generated donor-matched iMSCs and primary MSCs from three BM donors and compared their cell surface marker expression, proliferation potential, transcriptome, secretome and immunosuppressive properties (125). They showed that primary BM-MSCs expressed CD105 between 96.5 to 98.8%, CD90 between 93.5% to 98.3%, CD73 between 96.9 to 97.9% and CD34/CD45 between 0.33 to 0.52%. On the other hand, iMSCs expressed CD105 between 83.1-87.5%, CD90 between 74.5-86%, CD73 between 83.7-88.9% and CD34/CD45 between 0.25-2.28%. This result is similar to what we found in our studies where the iMSCs did not meet the ISCT criteria for CD90 (61.4%) and CD105 (74.5%). The study also found that the three autologous iMSCs had higher proliferation potential and longer telomere length than their parental MSCs. The authors concluded that since the iMSCs transcriptome was segregated from BM-MSCs, iMSCs are a distinct entity from their parental MSCs (125).

Our group previously led a modified Delphi study to establish and implement a consensus definition for MSCs and develop reporting guidelines for MSC clinical studies (129). In this study,

it was recognized that since there is no specific marker for MSCs and a combination of markers are used instead, there is a need for flexibility since MSCs markers vary depending on tissue origin and *in vitro* culture expansion. Therefore, the participants recommended that the flow cytometry results with the % of positive cells should be described for each positive and negative marker while always reporting CD45- as a negative cell surface marker to ensure the absence of contamination with hematopoietic lineage populations. Thus, it could be argued that the reason why the iMSCs did not meet the ISCT criteria is because these criteria were proposed in 2006 and new advancements in tissue sources and culture methods have significantly evolved since then.

As such, although the iMSCs did not meet the ISCT criteria, we still decided to test them *in vivo* to find out if they provide any therapeutic effects. Interestingly, the iMSCs offered therapeutic benefits on survival and RVH in the first experiment which was also reflected on the combined results of the three iMSC experiments **(Figure 10 and 14**). In contrast, UC-MSCs showed inter-donor variability in providing therapeutic effects where Donor 5 improved RVH while Donor 4 and 6 did not **(Figure 14)**. These results align with our hypothesis which states that the iMSCs are more likely to provide consistent and reliable treatment effects as opposed to UC-MSCs. In addition, this result supports the consensus from our group's Delphi study which states that flexibility in meeting the ISCT criteria for MSC markers is important since there are no specific markers for MSCs.

To better understand the mechanism of action of iMSCs and UC-MSCs, we decided to measure their IDO expression following exposure to IFN-γ. This test is known to cause the release of IDO by MSCs and has been proposed as a marker of MSCs' immunomodulatory potency (42). Our results showed that although all the cells met the minimum criteria of IDO expression for clinical trials, the iMSCs had the least increase in IDO expression **(Supplementary Figure 5)**.

Since this experiment was done only once, it is necessary to repeat it before determining whether or not this potency assay could predict the *in vivo* effects of MSCs.

Lee et al. suggested that iMSCs have a unique therapeutic potential distinct from their parental MSCs (125). They showed that the proteomic and transcriptomic profile of iMSCs demonstrated a significant increase in biological processes such as blood vessel development and increased pericyte markers such as NESTIN and CD146. Therefore, the authors concluded that the reprogramming of MSCs to iMSCs caused their cell fate to change towards a pericyte-like phenotype. Furthermore, the secretome of iMSCs were enriched with PDGF (platelet derived growth factor), endostatin, endothelin-1, BDNF (brain-derived neurotrophic factor), EGF (epidermal growth factor), and thrombostatin-2 (>2 folds compared to their parental MSCs) (125). In the light of this study and our results which showed that iMSCs were superior to most UC-MSCs in improving RVH and PAAT/PAET, we believe that their efficacy may be attributed to their enhanced ability to support blood vessel development through the production of angiogenic factors.

6. Future directions

Overall, our work sheds light on the ongoing challenge with inter-donor variability within UC-MSCs while simultaneously proposing iMSCs as a potential solution to this problem. However, further studies are required to further characterize those iMSCs and find their mechanism of action.

One method to better characterize the iMSCs would be through scRNA-seq which would allow us to compare the transcriptomic profiles of iMSCs and UC-MSCs, identify the top hit differentially expressed genes and subpopulations within each MSC type, revealing unique or shared clusters. Additional characterization methods include testing the differentiation, angiogenic and wound healing capacities of UC-MSCs and iMSCs. These methods will provide us with insights on their mechanism of action.

An area of improvement is potentially creating a more inflammatory and severe hyperoxia-induced lung injury model that better recapitulates the phenotype of BPD. Although the hyperoxia model has been routinely used in our lab to test new therapeutics, we believe that it is often moderate in severity and inconsistent. This is evident in the variability of survival and RVH severity across different experiments. To make a more severe model that better mimics BPD, our lab has established a 2HIT model that adds a hit of lipopolysaccharide (LPS) to a hyperoxia-induced model in neonatal mice (130). However, we are now interested in establishing a similar model in rats. Given that the iMSCs and UC-MSCs improved RVH in the hyperoxia-induced lung injury model, it would be interesting to see how the cells behave in a more inflammatory model due to the addition of LPS.

Given that so far we tested iMSCs from a single donor, it would be important to test iMSCs from additional donors to determine whether the effect seen in our experiments could be generalized to multiple iMSCs. We could assess the similarity of transcriptomes of iMSCs from different donors to find out if they exhibit inter-donor heterogeneity as seen in UC-MSCs. We could also study the cargo of EVs derived from iMSCs and UC-MSCs using mass spectrometry to identify their secretomes and in turn, better understand their mechanisms of action. Finally, it is worthwhile to test the effect of iMSC EVs in our model as collecting EVs could be an effective method of concentrating the therapeutic effect of MSCs, making a possibly more potent treatment.

7. Conclusion

This thesis explored iMSCs from a single donor as a new approach to provide consistent and scalable therapies for patients with BPD, the most frequent complication of prematurity. Here, we compared iMSCs against three different UC-MSCs (each isolated from a different donor). We demonstrated that the iMSCs improved RVH to the same extent in each experiment whereas UC-MSCs from different donors provided various levels of therapeutic effects. In addition, when we combined the data from those three experiments, we showed that the iMSCs not only improved RVH, but also improved PAAT/PAET, supporting the idea that iMSCs are superior to UC-MSCs in reducing PH, a serious complication of BPD which leads to high morbidity and mortality rates in premature infants.

7. Appendix

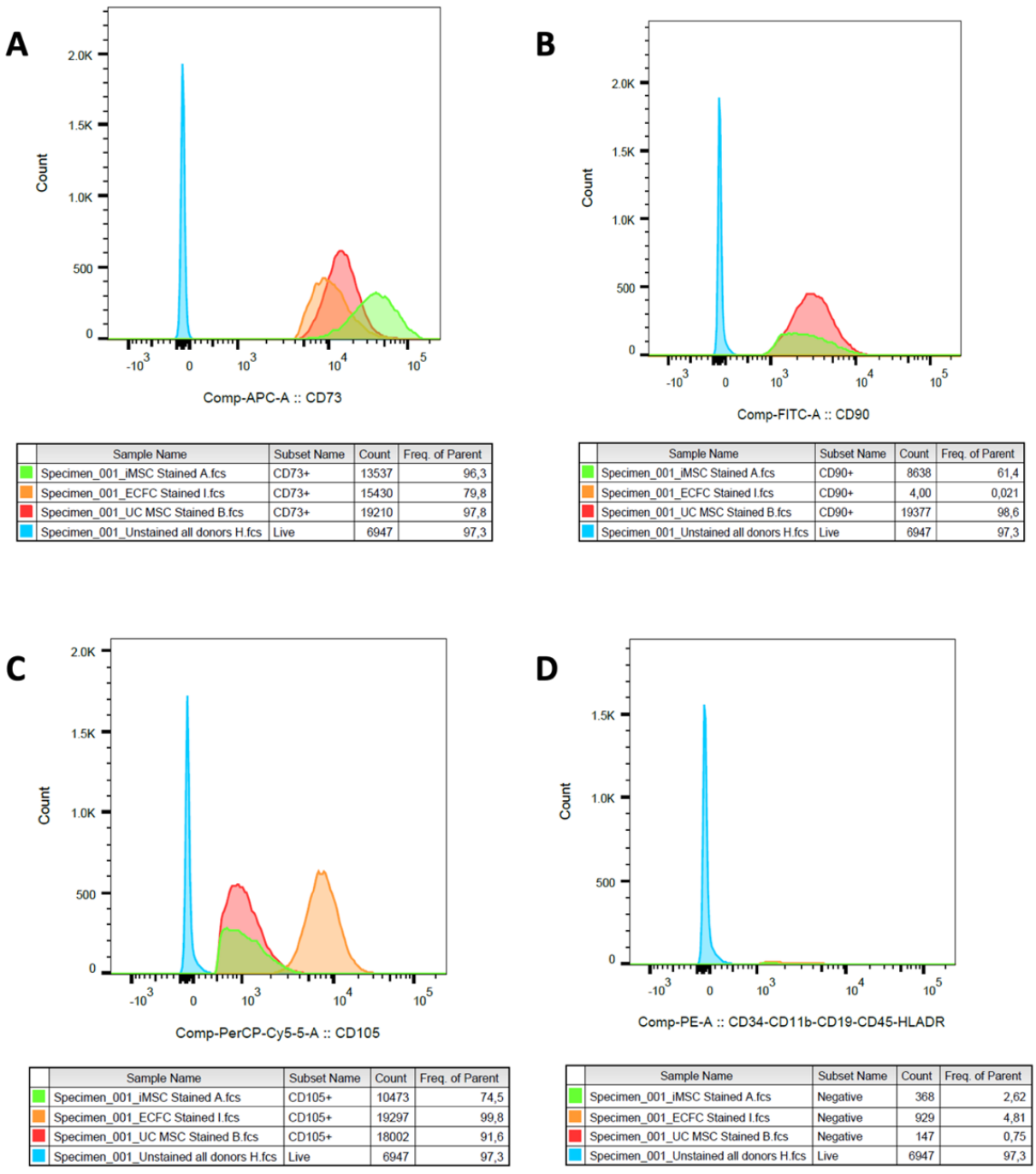

Sample Name	Subset Name	Count	Freq. of Parent
Specimen_001_iMSC Stained A.fcs	CD73+	13537	96,3
Specimen_001_ECFC Stained I.fcs	CD73+	15430	79,8
Specimen_001_UC MSC Stained B.fcs	CD73+	19210	97,8
Specimen_001_Unstained all donors H.fcs	Live	6947	97,3

Sample Name	Subset Name	Count	Freq. of Parent
Specimen_001_iMSC Stained A.fcs	CD90+	8638	61,4
Specimen_001_ECFC Stained I.fcs	CD90+	4,00	0,021
Specimen_001_UC MSC Stained B.fcs	CD90+	19377	98,6
Specimen_001_Unstained all donors H.fcs	Live	6947	97,3

Sample Name	Subset Name	Count	Freq. of Parent
Specimen_001_iMSC Stained A.fcs	CD105+	10473	74,5
Specimen_001_ECFC Stained I.fcs	CD105+	19297	99,8
Specimen_001_UC MSC Stained B.fcs	CD105+	18002	91,6
Specimen_001_Unstained all donors H.fcs	Live	6947	97,3

Sample Name	Subset Name	Count	Freq. of Parent
Specimen_001_iMSC Stained A.fcs	Negative	368	2,62
Specimen_001_ECFC Stained I.fcs	Negative	929	4,81
Specimen_001_UC MSC Stained B.fcs	Negative	147	0,75
Specimen_001_Unstained all donors H.fcs	Live	6947	97,3

Supplementary Figure 1. Characterizing iMSCs using flow cytometry to detect the expression of CD90, CD105, CD73, CD11b-CD34-CD11b-CD19-CD45-HLA-DR compared to UC-MSCs (positive control) and ECFCs (negative control). (A) iMSCs (P4), ECFCs (P3) and UC-MSCs (P3) were used for flow cytometry analyses, and the values represent the percentage

of positive cells for CD73 (96.3, 79.8 and 97.8, respectively). **(B)** The values represent the percentage of positive iMSCs (P4), ECFCs (P3) and UC-MSCs (P3) for CD90 (61.4, 0.021 and 98.6, respectively). **(C)** The values represent the percentage of positive iMSCs (P4), ECFCs (P3) and UC-MSCs (P3) for CD105 (74.5, 99.8 and 91.6, respectively). **(D)** The values represent the percentage of positive iMSCs (P4), ECFCs (P3) and UC-MSCs (P3) for CD11b-CD34-CD11b-CD19-CD45-HLA-DR (2.62, 4.81 and 0.75, respectively).

A

Surface marker	Donor 4	Donor 5	Donor 6
CD73	100%	100%	99.7%
CD90	99.2%	100%	99.6%
CD105	99.6%	99.9%	99.0%
CD14	0.14%	0.16%	0.49%
CD19	0.06%	0.34%	0.01%
CD34	0.05%	0.09%	0.13%
CD45	0.45%	0.59%	0.54%
HLA-DR	0.08%	0.56%	0.12%

B

Cell Bank Criteria	Donor 4	Donor 5	Donor 6
Doubling time	22.6	21.9	25.8
% Viability post-thaw (Trypan blue)	95.3%	97.2%	95.1%
Endotoxin Levels (EU/mL)	< 0.05	<0.05	< 0.05
BACTEC Sterility (Aerobic and Anaerobic Bacterial growth)	No Growth	No Growth	No Growth
Mycoplasma	Negative	Negative	Negative
Potency Assay – CFU Assay	Growth	Growth	Growth
Potency Assay – IDO Expression (ΔΔCq)	14.77	15.04	14.68

Supplementary Figure 2. Characterization of Donor 4, 5 and 6 UC-MSCs from the CMF. **(A)** Cell surface marker expression of CD73, CD90, CD105, CD14, CD19, CD34, CD45 and HLA-DR. **(B)** Doubling time, % viability post-thaw, endotoxin levels, BACTEC sterility, mycoplasma, CFU assay and IDO expression results.

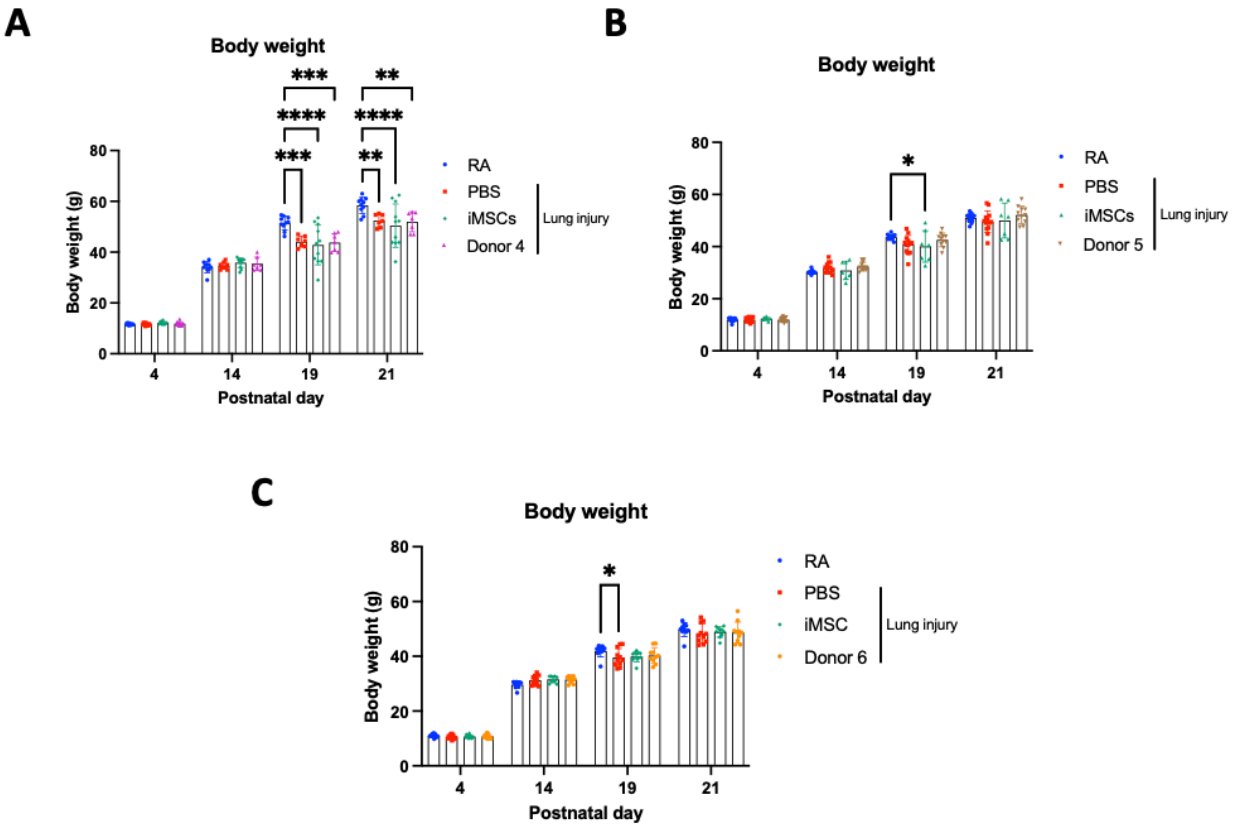

Supplementary Figure 3. Body weight differences at P4, P14, P19 and P21. (A) iMSC and Donor 4 experiment body weight (g) at P4, P14, P19 and P21 (RA untreated; n=10, O2 + PBS; n=7, O2 + iMSCs; n=11, O2 + Donor 4 UC-MSCs; n=7). **(B)** iMSC and Donor 5 experiment body weight (g) at P4, P14, P19 and P21 (RA untreated; n=12, O2 + PBS; n=13, O2 + iMSCs; n=7, O2 + Donor 5 UC-MSCs; n=11). **(C)** iMSC and Donor 6 experiment body weight (g) at P4, P14, P19 and P21 (RA untreated; n=10, O2 + PBS; n=11, O2 + iMSCs; n=10, O2 + Donor 6 UC-MSCs; n=10). Values are represented as the mean ± STD. Statistical analysis: ordinary one-way ANOVA with Tukey's multiple comparison post hoc test; *: $p \leq 0.05$, **: $p \leq 0.01$, ***: $p \leq 0.001$, and ****: $p \leq 0.0001$. Individual rats represented by each dot.

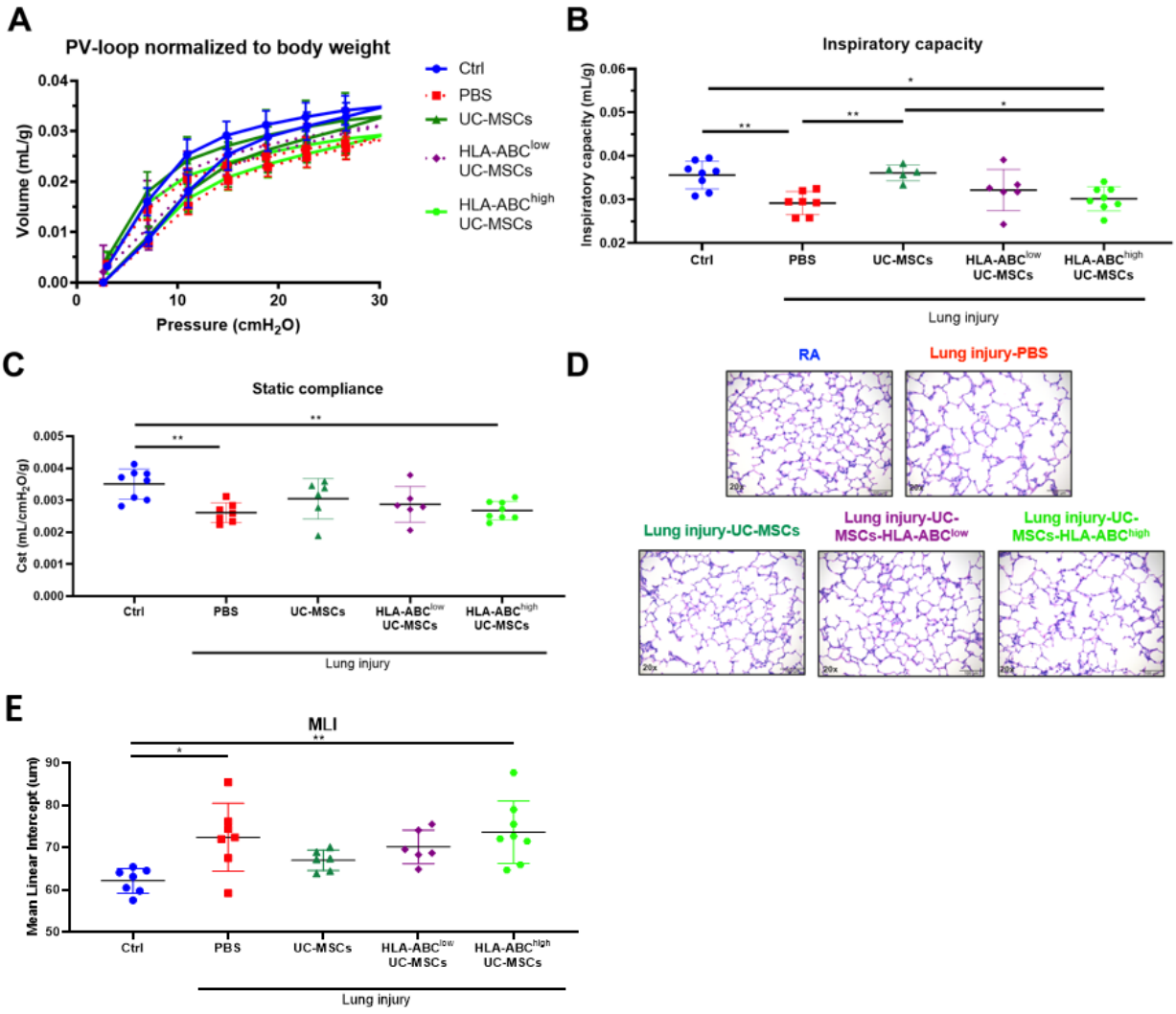

Supplementary Figure 4. UC-MSCs expressing high levels of HLA-A,-B,-C do not improve lung structure or lung function. (A) Body weight-adjusted pressure volume (PV)-loops curves where each loop represents the mean lung volume of all pups within one group at each pressure point (RA untreated; n=8 in (B) and (C) and n=7 (1 outlier) in (E), O2 + PBS; n=7, O2 + full population of UC-MSCs; n=5 (1 outlier) in (B) and n=6 in (C) and (E), O2 + UC-MSCs HLA-A,-B,-C low; n=6 and O2 + UC-MSCs HLA-A,-B,-C high; n=8). **(B)** Body weight-adjusted inspiratory capacity (mL/g). **(C)** Body weight-adjusted static compliance (Cst). **(D)** Representative images of H&E- stained lung sections. **(E)** Quantification of MLI as a proxy for mean diameter of alveoli in lung tissue section from RA, O2 + PBS, O2 + full population of UC-MSCs, O2 + UC-MSCs HLA-A,-B,-C low and O2 + UC-MSCs HLA-A,-B,-C high. Individual rats represented by each dot (n=5-8 per group). Values are represented as the mean ± STD. Significant results calculated by ordinary one-way ANOVA with Tukey's multiple comparison post hoc test. *: $p \leq 0.05$, **: $p \leq 0.01$, ***: $p \leq 0.001$, and ****: $p \leq 0.0001$.

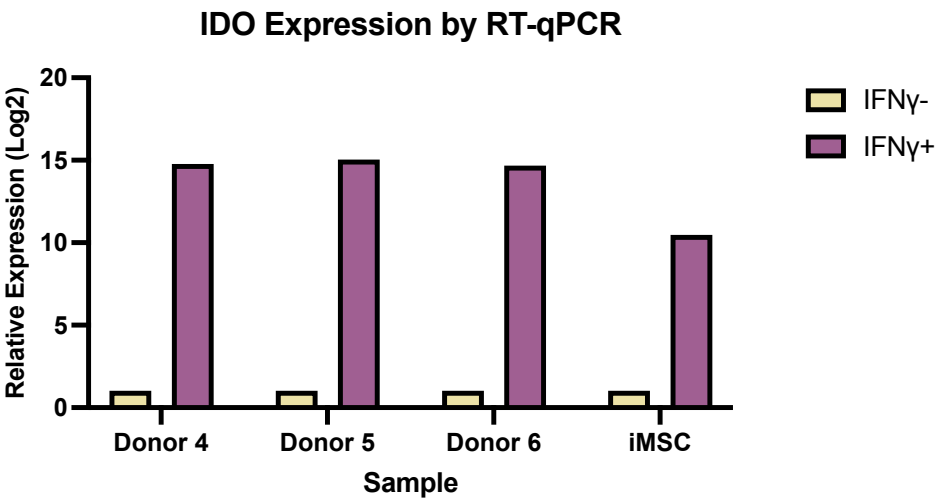

Supplementary Figure 5. Assess the immunosuppressive potential of UC-MSCs and iMSCs by determining mRNA relative expression of IDO after stimulation with IFNγ for 24h. mRNA expression levels of IDO were measured by RT-qPCR from Donors 4, 5 and 6 UC-MSCs at PN1 and iMSCs at PN2. Unstimulated UC-MSCs and iMSCs at the corresponding passage were used as control

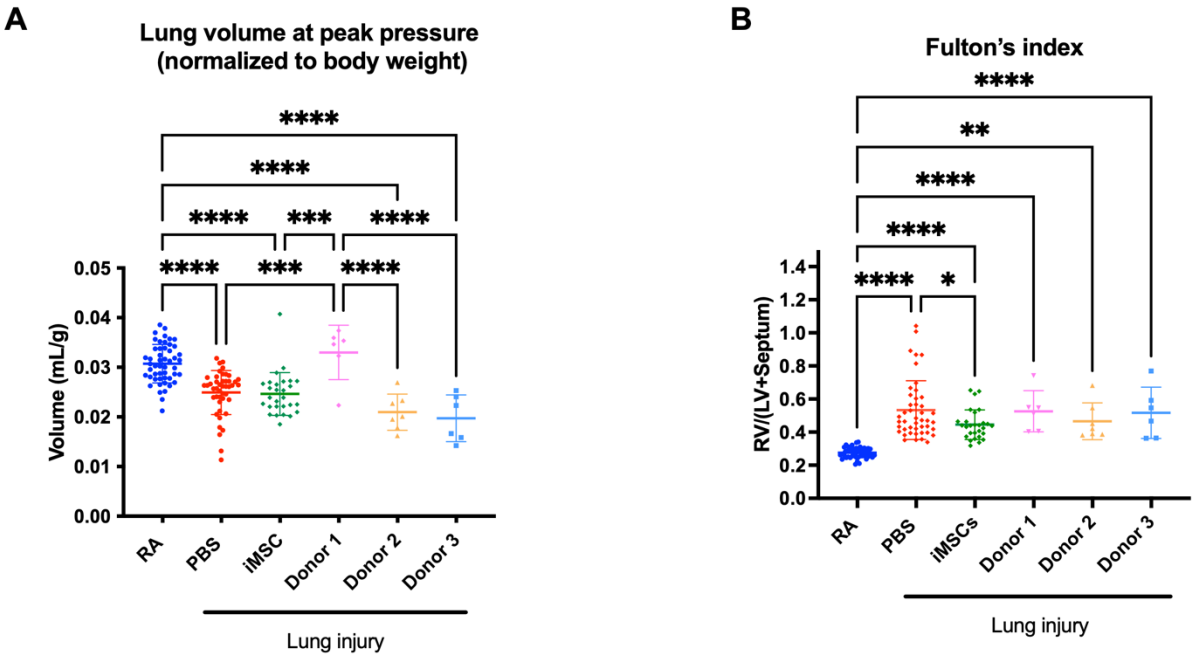

Supplementary Figure 6. Treatment with UC-MSCs isolated from Donor 1, but not Donor 2 and 3 or iMSCs, improved lung function in a hyperoxia-induced rat BPD model. (A) Body weight-adjusted inspiratory capacity (mL/g) (RA untreated; n=50, O2 + PBS; n=45, Donor 1; n=6

and O2 + Donor 2; n=7, Donor 3; n=6, iMSCs; n=28). **(B)** Fulton's index quantifying right ventricular hypertrophy (RA untreated; n=50, O2 + PBS; n=45, Donor 1; n=6 and O2 + Donor 2; n=7, Donor 3; n=6, iMSCs; n=28). Individual rats are represented by each dot. Values are represented as the mean ± STD. Significant results calculated by ordinary one-way ANOVA with Tukey's multiple comparison post hoc test. *: $p \leq 0.05$, **: $p \leq 0.01$, ***: $p \leq 0.001$, and ****: $p \leq 0.0001$.

8. References

1. Thébaud B, Goss KN, Laughon M, Whitsett JA, Abman SH, Steinhorn RH, et al. Bronchopulmonary dysplasia HHS Public Access. Nat Rev Dis Primers. 2019;5:1–23.
2. Stoll BJ, Hansen NI, Bell EF, Walsh MC, Carlo WA, Shankaran S, et al. Trends in Care Practices, Morbidity, and Mortality of Extremely Preterm Neonates, 1993-2012. JAMA. 2015 Sep 8;314(10):1039–51.
3. Siffel C, Kistler KD, Lewis JFM, Sarda SP. Global incidence of bronchopulmonary dysplasia among extremely preterm infants: a systematic literature review. Journal of Maternal-Fetal and Neonatal Medicine. 2021;34(11):1721–31.
4. Jobe AJ. The New BPD: An Arrest of Lung Development. Pediatric Research 1999 46:6. 1999;46(6):641–641.
5. Northway WH, RRC, and PDY. Pulmonary Disease Following Respirator Therapy of Hyaline-membrane Disease. 1967;276:357–68.
6. Abman SH, Bancalari E, Jobe A. The Evolution of Bronchopulmonary Dysplasia after 50 Years. Am J Respir Crit Care Med. 2017 Feb 15;195(4):421–4.
7. Lavoie PM, Pham C, Jang KL. Heritability of bronchopulmonary dysplasia, defined according to the consensus statement of the National Institute of Health. Pediatrics. 2008;122(3):479–85.
8. Parker RA, Lindstrom DP, Cotton RB. Evidence from Twin Study Implies Possible Genetic Susceptibility to Bronchopulmonary Dysplasia. Semin Perinatol. 1996;20(3):206–9.
9. Hansen AR, Barnés CM, Folkman J, McElrath TF. Maternal preeclampsia predicts the development of bronchopulmonary dysplasia. J Pediatr. 2010 Apr;156(4):532–6.
10. Kim CJ, Romero R, Chaemsaithong P, Chaiyasit N, Yoon BH, Kim YM. Acute chorioamnionitis and funisitis: definition, pathologic features, and clinical significance. Am J Obstet Gynecol. 2015 Oct 1;213(4 Suppl):S29–52.
11. Jobe AH. Mechanisms of Lung Injury and Bronchopulmonary Dysplasia. Am J Perinatol. 2016;33:1076–8.
12. Hurskainen M, Mižíková I, Cook DP, Andersson N, Cyr-Depauw C, Lesage F, et al. Single cell transcriptomic analysis of murine lung development on hyperoxia-induced damage. Nature Communications 2021 12:1 [Internet]. 2021 Mar 10 [cited 2025 Jun 21];12(1):1–19. Available from: https://www.nature.com/articles/s41467-021-21865-2
13. Arora S, Dev K, Agarwal B, Das P, Syed MA. Macrophages: Their role, activation and polarization in pulmonary diseases. Immunobiology [Internet]. 2018 Apr 1 [cited 2025 Jun 21];223(4–5):383–96. Available from: https://pubmed.ncbi.nlm.nih.gov/29146235/

14. Wong PM, Lees AN, Louw J, Lee FY, French N, Gain K, et al. Emphysema in young adult survivors of moderate-to-severe bronchopulmonary dysplasia. European Respiratory Journal. 2008 Aug;32(2):321–8.

15. Mourani PM, Dunbar Ivy D, Rosenberg AA, Fagan TE, Abman SH. Left Ventricular Diastolic Dysfunction in Bronchopulmonary Dysplasia. J Pediatr. 2008;152(2):291–3.

16. Goss KN, Beshish AG, Barton GP, Haraldsdottir K, Levin TS, Tetri LH, et al. Early Pulmonary Vascular Disease in Young Adults Born Preterm. Am J Respir Crit Care Med. 2018 Dec 15;198(12):1549–58.

17. Landry JS, Chan T, Lands L, Menzies D. Long-term impact of bronchopulmonary dysplasia on pulmonary function. Can Respir J. 18(5):514–843.

18. Schmidt B, Roberts RS, Davis P, Doyle LW, Barrington KJ, Ohlsson A, et al. Long-term effects of caffeine therapy for apnea of prematurity. N Engl J Med. 2007 Nov 8;357(19):1893–902.

19. Kribs A, Roll C, Göpel W, Wieg C, Groneck P, Laux R, et al. Nonintubated Surfactant Application vs Conventional Therapy in Extremely Preterm Infants: A Randomized Clinical Trial. JAMA Pediatr. 2015 Aug 1;169(8):723–30.

20. Dargaville PA, Aiyappan A, De Paoli AG, Kuschel CA, Kamlin COF, Carlin JB, et al. Minimally-invasive surfactant therapy in preterm infants on continuous positive airway pressure. Arch Dis Child Fetal Neonatal Ed. 2013;98(2).

21. Aldana-Aguirre JC, Pinto M, Featherstone RM, Kumar M. Less invasive surfactant administration versus intubation for surfactant delivery in preterm infants with respiratory distress syndrome: a systematic review and meta-analysis. Arch Dis Child Fetal Neonatal Ed. 2017 Jan 1;102(1):F17–23.

22. Darlow BA, Graham PJ, Rojas-Reyes MX. Vitamin A supplementation to prevent mortality and short- and long-term morbidity in very low birth weight infants. Cochrane Database Syst Rev. 2016 Aug 22;2016(8).

23. Baud O, Trousson C, Biran V, Leroy E, Mohamed D, Alberti C. Association Between Early Low-Dose Hydrocortisone Therapy in Extremely Preterm Neonates and Neurodevelopmental Outcomes at 2 Years of Age. JAMA. 2017 Apr 4;317(13):1329–37.

24. Thébaud B, Goss KN, Laughon M, Whitsett JA, Abman SH, Steinhorn RH, et al. Bronchopulmonary dysplasia. Nature Reviews Disease Primers 2019 5:1 [Internet]. 2019 Nov 14 [cited 2023 Apr 11];5(1):1–23. Available from: https://www.nature.com/articles/s41572-019-0127-7

25. Behrman RE, Butler AStith, Institute of Medicine (U.S.). Committee on Understanding Premature Birth and Assuring Healthy Outcomes. Preterm birth : causes, consequences, and prevention. Vol. 10. National Academies Press; 2007. 313–345 p.

26. Perin HJ, Yeung MSPH D, Villavicencio F, Black RE, Liu L, Mulick A, et al. Global, regional, and national causes of under-5 mortality in 2000-19: an updated systematic analysis with implications for the Sustainable Development Goals. Lancet Child Adolesc Health. 2022;6:106–21.

27. Walani SR. Global burden of preterm birth. Vol. 150, International Journal of Gynecology and Obstetrics. John Wiley and Sons Ltd.; 2020. p. 31–3.

28. O'reilly M, Thébaud B. Animal models of bronchopulmonary dysplasia. The term rat models. Am J Physiol Lung Cell Mol Physiol. 2014;307:948–58.

29. Shaffer SG, O'Neill D, Bradt SK, Thibeault DW. Chronic vascular pulmonary dysplasia associated with neonatal hyperoxia exposure in the rat. Pediatr Res. 1987;21(1):14–20.

30. Pittenger MF, Mackay AM, Beck SC, Jaiswal RK, Douglas R, Mosca JD, et al. Multilineage potential of adult human mesenchymal stem cells. Science (1979) [Internet]. 1999 Apr 2 [cited 2025 Apr 17];284(5411):143–7. Available from: https://www.science.org/doi/10.1126/science.284.5411.143

31. Till JE, McCulloch EA. A direct measurement of the radiation sensitivity of normal mouse bone marrow cells. 1961. Radiat Res. 2011 Feb;175(2):145–9.

32. Pittenger MF, Discher DE, Péault BM, Phinney DG, Hare JM, Caplan AI. Mesenchymal stem cell perspective: cell biology to clinical progress. Vol. 4, npj Regenerative Medicine. Nature Research; 2019.

33. Dominici M, Le Blanc K, Mueller I, Slaper-Cortenbach I, Marini FC, Krause DS, et al. Minimal criteria for defining multipotent mesenchymal stromal cells. The International Society for Cellular Therapy position statement. Cytotherapy. 2006 Aug;8(4):315–7.

34. Nagamura-Inoue T, He H. Umbilical cord-derived mesenchymal stem cells: Their advantages and potential clinical utility. World J Stem Cells. 2014 Apr 4;6(2):195.

35. Li T, Xia M, Gao Y, Chen Y, Xu Y. Human umbilical cord mesenchymal stem cells: An overview of their potential in cell-based therapy. Vol. 15, Expert Opinion on Biological Therapy. Taylor and Francis Ltd.; 2015. p. 1293–306.

36. Namba F. Mesenchymal stem cells for the prevention of bronchopulmonary dysplasia. Vol. 61, Pediatrics International. Blackwell Publishing; 2019. p. 945–50.

37. Maitra B, Szekely E, Gjini K, Laughlin MJ, Dennis J, Haynesworth SE, et al. Human mesenchymal stem cells support unrelated donor hematopoietic stem cells and suppress T-cell activation. Bone Marrow Transplant [Internet]. 2004 Mar [cited 2025 Mar 13];33(6):597–604. Available from: https://pubmed.ncbi.nlm.nih.gov/14716336/

38. Ge W, Jiang J, Arp J, Liu W, Garcia B, Wang H. Regulatory T-cell generation and kidney allograft tolerance induced by mesenchymal stem cells associated with indoleamine 2,3-dioxygenase expression. Transplantation [Internet]. 2010 Dec 27 [cited 2025 Mar 13];90(12):1312–20. Available from: https://pubmed.ncbi.nlm.nih.gov/21042238/

39. Sato K, Ozaki K, Oh I, Meguro A, Hatanaka K, Nagai T, et al. Nitric oxide plays a critical role in suppression of T-cell proliferation by mesenchymal stem cells. Blood [Internet]. 2007 Jan 1 [cited 2025 Mar 13];109(1):228–34. Available from: https://pubmed.ncbi.nlm.nih.gov/16985180/

40. Wu R, Liu C, Deng X, Chen L, Hao S, Ma L. Enhanced alleviation of aGVHD by TGF-β1-modified mesenchymal stem cells in mice through shifting MΦ into M2 phenotype and promoting the differentiation of Treg cells. J Cell Mol Med [Internet]. 2019 Jan 1 [cited 2025 Mar 13];24(2):1684. Available from: https://pmc.ncbi.nlm.nih.gov/articles/PMC6991663/

41. Ren G, Zhang L, Zhao X, Xu G, Zhang Y, Roberts AI, et al. Mesenchymal stem cell-mediated immunosuppression occurs via concerted action of chemokines and nitric oxide. Cell Stem Cell [Internet]. 2008 Feb 7 [cited 2025 Mar 13];2(2):141–50. Available from: https://pubmed.ncbi.nlm.nih.gov/18371435/

42. Boyt DT, Boland LK, Burand AJ, Brown AJ, Ankrum JA. Dose and duration of interferon γ pre-licensing interact with donor characteristics to influence the expression and function of indoleamine-2,3-dioxygenase in mesenchymal stromal cells. J R Soc Interface [Internet]. 2020 Jun 1 [cited 2025 Mar 13];17(167). Available from: https://pubmed.ncbi.nlm.nih.gov/32546114/

43. Wu X, Jiang J, Gu Z, Zhang J, Chen Y, Liu X. Mesenchymal stromal cell therapies: immunomodulatory properties and clinical progress. Stem Cell Research & Therapy 2020 11:1 [Internet]. 2020 Aug 8 [cited 2025 Mar 13];11(1):1–16. Available from: https://stemcellres.biomedcentral.com/articles/10.1186/s13287-020-01855-9

44. Islam MN, Das SR, Emin MT, Wei M, Sun L, Westphalen K, et al. Mitochondrial transfer from bone-marrow-derived stromal cells to pulmonary alveoli protects against acute lung injury. Nat Med [Internet]. 2012 May [cited 2025 Mar 15];18(5):759–65. Available from: https://pubmed.ncbi.nlm.nih.gov/22504485/

45. Willis GR, Fernandez-Gonzalez A, Anastas J, Vitali SH, Liu X, Ericsson M, et al. Mesenchymal stromal cell exosomes ameliorate experimental bronchopulmonary dysplasia and restore lung function through macrophage immunomodulation. Am J Respir Crit Care Med [Internet]. 2018 Jan 1 [cited 2025 Mar 15];197(1):104–16. Available from: www.atsjournals.org.

46. Hurskainen M, Cyr-Depauw C, Thébaud B. Insights into the mechanisms of alveolarization - Implications for lung regeneration and cell therapies. Semin Fetal Neonatal Med. 2022 Feb 1;27(1):101243.

47. Xi J, Yan X, Zhou J, Yue W, Pei X. Mesenchymal stem cells in tissue repairing and regeneration: Progress and future. Vol. 1, Burns and Trauma. Oxford University Press; 2013. p. 13–20.

48. Pitt JM, Kroemer G, Zitvogel L. Extracellular vesicles: masters of intercellular communication and potential clinical interventions. J Clin Invest. 2016 Apr 4;126(4):1139.

49. El Andaloussi S, Mäger I, Breakefield XO, Wood MJA. Extracellular vesicles: biology and emerging therapeutic opportunities. Nature Reviews Drug Discovery 2013 12:5. 2013 Apr 15;12(5):347–57.

50. Phinney DG, Pittenger MF. Concise Review: MSC-Derived Exosomes for Cell-Free Therapy. Stem Cells. 2017 Apr 1;35(4):851–8.

51. Heijnen HFG, Schiel AE, Fijnheer R, Geuze HJ, Sixma JJ. Activated Platelets Release Two Types of Membrane Vesicles: Microvesicles by Surface Shedding and Exosomes Derived From Exocytosis of Multivesicular Bodies and α-Granules. Blood. 1999 Dec 1;94(11):3791–9.

52. Augustine S, Avey MT, Harrison B, Locke T, Ghannad M, Moher D, et al. Mesenchymal Stromal Cell Therapy in Bronchopulmonary Dysplasia: Systematic Review and Meta-Analysis of Preclinical Studies. Stem Cells Transl Med. 2017 Dec 1;6(12):2079–93.

53. Murphy DE, de Jong OG, Brouwer M, Wood MJ, Lavieu G, Schiffelers RM, et al. Extracellular vesicle-based therapeutics: natural versus engineered targeting and trafficking. Experimental & Molecular Medicine 2019 51:3 [Internet]. 2019 Mar 15 [cited 2025 May 1];51(3):1–12. Available from: https://www.nature.com/articles/s12276-019-0223-5

54. Tieu A, Stewart DJ, Chwastek D, Lansdell C, Burger D, Lalu MM. Biodistribution of mesenchymal stromal cell-derived extracellular vesicles administered during acute lung injury. Stem Cell Res Ther [Internet]. 2023 Dec 1 [cited 2025 May 1];14(1). Available from: https://pubmed.ncbi.nlm.nih.gov/37705086/

55. Barreca MM, Cancemi P, Geraci F. Mesenchymal and Induced Pluripotent Stem Cells-Derived Extracellular Vesicles: The New Frontier for Regenerative Medicine? Vol. 9, Cells. NLM (Medline); 2020.

56. Lesage F, Thébaud B. Mesenchymal Stromal Cell-Derived Extracellular Vesicles for Neonatal Lung Disease: Tiny Particles, Major Promise, Rigorous Requirements for Clinical Translation. Cells 2022, Vol 11, Page 1176. 2022 Mar 31;11(7):1176.

57. Willis GR, Fernandez-Gonzalez A, Reis M, Yeung V, Liu X, Ericsson M, et al. Mesenchymal stromal cell-derived small extracellular vesicles restore lung architecture and improve exercise capacity in a model of neonatal hyperoxia-induced lung injury. J Extracell Vesicles. 2020 Jan 1;9(1).

58. Fujii S, Miura Y, Fujishiro A, Shindo T, Shimazu Y, Hirai H, et al. Graft-Versus-Host Disease Amelioration by Human Bone Marrow Mesenchymal Stromal/Stem Cell-Derived Extracellular Vesicles Is Associated with Peripheral Preservation of Naive T Cell Populations. Stem Cells. 2018 Mar 1;36(3):434–45.

59. Burrello J, Monticone S, Gai C, Gomez Y, Kholia S, Camussi G. Stem Cell-Derived Extracellular Vesicles and Immune-Modulation. Front Cell Dev Biol. 2016 Aug 22;4(AUG).

60. Kordelas L, Rebmann V, Ludwig AK, Radtke S, Ruesing J, Doeppner TR, et al. MSC-derived exosomes: A novel tool to treat therapy-refractory graft-versus-host disease. Vol. 28, Leukemia. Nature Publishing Group; 2014. p. 970–3.

61. Sengupta V, Sengupta S, Lazo A, Woods P, Nolan A, Bremer N. Exosomes Derived from Bone Marrow Mesenchymal Stem Cells as Treatment for Severe COVID-19. Stem Cells Dev. 2020 Jun 15;29(12):747–54.

62. Panés J, García-Olmo D, Van Assche G, Colombel JF, Reinisch W, Baumgart DC, et al. Expanded allogeneic adipose-derived mesenchymal stem cells (Cx601) for complex perianal fistulas in Crohn's disease: a phase 3 randomised, double-blind controlled trial. The Lancet [Internet]. 2016 Sep 24 [cited 2025 Jan 3];388(10051):1281–90. Available from: http://www.thelancet.com/article/S014067361631203X/fulltext

63. Martin PJ, Uberti JP, Soiffer RJ, Klingemann H, Waller EK, Daly AS, et al. Prochymal Improves Response Rates In Patients With Steroid-Refractory Acute Graft Versus Host Disease (SR-GVHD) Involving The Liver And Gut: Results Of A Randomized, Placebo-Controlled, Multicenter Phase III Trial In GVHD. Biology of Blood and Marrow Transplantation [Internet]. 2010 Feb 1 [cited 2025 Jan 3];16(2):S169–70. Available from: http://www.astctjournal.org/article/S1083879109006533/fulltext

64. Whitfield MJ, Lee WCJ, Van Vliet KJ. Onset of heterogeneity in culture-expanded bone marrow stromal cells. Stem Cell Res. 2013 Nov;11(3):1365–77.

65. McLeod CM, Mauck RL. On the origin and impact of mesenchymal stem cell heterogeneity: new insights and emerging tools for single cell analysis. Eur Cell Mater. 2017 Oct 27;34:217–31.

66. Costa LA, Eiro N, Fraile M, Gonzalez LO, Saá J, Garcia-Portabella P, et al. Functional heterogeneity of mesenchymal stem cells from natural niches to culture conditions: implications for further clinical uses. Cellular and Molecular Life Sciences. 2021 Jan 1;78(2):447–67.

67. Baksh D, Yao R, Tuan RS. Comparison of proliferative and multilineage differentiation potential of human mesenchymal stem cells derived from umbilical cord and bone marrow. Stem Cells [Internet]. 2007 Jun 1 [cited 2025 Mar 20];25(6):1384–92. Available from: https://pubmed.ncbi.nlm.nih.gov/17332507/

68. Goetz MJ, Kremer S, Behnke J, Staude B, Shahzad T, Holzfurtner L, et al. MSC Based Therapies to Prevent or Treat BPD—A Narrative Review on Advances and Ongoing Challenges. Int J Mol Sci. 2021 Feb 1;22(3):1–27.

69. Cyr-Depauw C, Cook DP, Mižik I, Lesage F, Vadivel A, Renesme L, et al. Single-Cell RNA Sequencing Reveals Repair Features of Human Umbilical Cord Mesenchymal Stromal Cells. Am J Respir Crit Care Med. 2024 Sep 15;

70. Kamerkar S, Lebleu VS, Sugimoto H, Yang S, Ruivo CF, Melo SA, et al. Exosomes facilitate therapeutic targeting of oncogenic KRAS in pancreatic cancer. Nature 2017 546:7659. 2017 Jun 7;546(7659):498–503.

71. Wen S, Dooner M, Cheng Y, Papa E, Del Tatto M, Pereira M, et al. Mesenchymal stromal cell-derived extracellular vesicles rescue radiation damage to murine marrow hematopoietic cells. Leukemia 2016 30:11. 2016 May 6;30(11):2221–31.

72. Didiot MC, Hall LM, Coles AH, Haraszti RA, Godinho BMDC, Chase K, et al. Exosome-mediated Delivery of Hydrophobically Modified siRNA for Huntingtin mRNA Silencing. Molecular Therapy. 2016 Oct 1;24(10):1836–47.

73. Pi F, Binzel DW, Lee TJ, Li Z, Sun M, Rychahou P, et al. Nanoparticle orientation to control RNA loading and ligand display on extracellular vesicles for cancer regression. Nature Nanotechnology 2017 13:1. 2017 Dec 11;13(1):82–9.

74. Tieu A, Hu K, Gnyra C, Montroy J, Fergusson DA, Allan DS, et al. Mesenchymal stromal cell extracellular vesicles as therapy for acute and chronic respiratory diseases: A meta-analysis. J Extracell Vesicles [Internet]. 2021 Oct 1 [cited 2025 May 1];10(12). Available from: https://pubmed.ncbi.nlm.nih.gov/34596349/

75. Potter M, Lins B, Mietzsch M, Heilbronn R, Van Vliet K, Chipman P, et al. A simplified purification protocol for recombinant adeno-associated virus vectors. Mol Ther Methods Clin Dev. 2014 Jan 1;1:14034.

76. Dizon-Maspat J, Bourret J, D'Agostini A, Li F. Single pass tangential flow filtration to debottleneck downstream processing for therapeutic antibody production. Biotechnol Bioeng. 2012 Apr 1;109(4):962–70.

77. Grimm KM, Trigona WL, Heidecker GJ, Joyce JG, Fu TM, Shiver JW, et al. An Enhanced and Scalable Process for the Purification of SIV Gag-Specific MHC Tetramer. Protein Expr Purif. 2001 Nov 1;23(2):270–81.

78. Gimona M, Pachler K, Laner-Plamberger S, Schallmoser K, Rohde E. Manufacturing of Human Extracellular Vesicle-Based Therapeutics for Clinical Use. International Journal of Molecular Sciences 2017, Vol 18, Page 1190. 2017 Jun 3;18(6):1190.

79. Zhou X, Liu J, Wu F, Mao J, Wang Y, Zhu J, et al. The application potential of iMSCs and iMSC-EVs in diseases. Front Bioeng Biotechnol [Internet]. 2024 [cited 2024 Aug 13];12. Available from: https://pubmed.ncbi.nlm.nih.gov/39135947/

80. Dupuis V, Oltra E. Methods to produce induced pluripotent stem cell-derived mesenchymal stem cells: Mesenchymal stem cells from induced pluripotent stem cells.

World J Stem Cells [Internet]. 2021 [cited 2025 Apr 17];13(8):1094. Available from: https://pmc.ncbi.nlm.nih.gov/articles/PMC8422924/

81. Li CL, Leng Y, Zhao B, Gao C, Du FF, Jin N, et al. Human iPSC-MSC-Derived Xenografts Modulate Immune Responses by Inhibiting the Cleavage of Caspases. Stem Cells [Internet]. 2017 Jul 1 [cited 2025 Jan 3];35(7):1719–32. Available from: https://dx.doi.org/10.1002/stem.2638

82. Wang LT, Jiang SS, Ting CH, Hsu PJ, Chang CC, Sytwu HK, et al. Differentiation of Mesenchymal Stem Cells from Human Induced Pluripotent Stem Cells Results in Downregulation of c-Myc and DNA Replication Pathways with Immunomodulation Toward CD4 and CD8 Cells. Stem Cells [Internet]. 2018 Jun 1 [cited 2025 Jan 3];36(6):903–14. Available from: https://dx.doi.org/10.1002/stem.2795

83. Giuliani M, Oudrhiri N, Noman ZM, Vernochet A, Chouaib S, Azzarone B, et al. Human mesenchymal stem cells derived from induced pluripotent stem cells down-regulate NK-cell cytolytic machinery. Blood [Internet]. 2011 Sep 22 [cited 2025 Jan 3];118(12):3254–62. Available from: https://dx.doi.org/10.1182/blood-2010-12-325324

84. Soontararak S, Chow L, Johnson V, Coy J, Wheat W, Regan D, et al. Mesenchymal Stem Cells (MSC) Derived from Induced Pluripotent Stem Cells (iPSC) Equivalent to Adipose-Derived MSC in Promoting Intestinal Healing and Microbiome Normalization in Mouse Inflammatory Bowel Disease Model. Stem Cells Transl Med [Internet]. 2018 Jun 1 [cited 2025 Jan 3];7(6):456–67. Available from: https://dx.doi.org/10.1002/sctm.17-0305

85. Liu B, Chen F, Wu Y, Wang X, Feng M, Li Z, et al. Enhanced tumor growth inhibition by mesenchymal stem cells derived from iPSCs with targeted integration of interleukin24 into rDNA loci. Oncotarget [Internet]. 2017 Mar 28 [cited 2025 Jan 3];8(25):40791–803. Available from: https://www.oncotarget.com/article/16584/text/

86. Cheng PP, Liu XC, Ma PF, Gao C, Li JL, Lin YY, et al. iPSC-MSCs Combined with Low-Dose Rapamycin Induced Islet Allograft Tolerance Through Suppressing Th1 and Enhancing Regulatory T-Cell Differentiation. https://home.liebertpub.com/scd [Internet]. 2015 Apr 13 [cited 2025 Jan 3];24(15):1793–804. Available from: https://www.liebertpub.com/doi/10.1089/scd.2014.0488

87. Zhong H, Fan XL, Fang S Bin, Lin YD, Wen W, Fu QL. Human pluripotent stem cell-derived mesenchymal stem cells prevent chronic allergic airway inflammation via TGF-β1-Smad2/Smad3 signaling pathway in mice. Mol Immunol. 2019 May 1;109:51–7.

88. Fang S Bin, Zhang HY, Wang C, He BX, Liu XQ, Meng XC, et al. Small extracellular vesicles derived from human mesenchymal stromal cells prevent group 2 innate lymphoid cell-dominant allergic airway inflammation through delivery of miR-146a-5p. J Extracell Vesicles [Internet]. 2020 Sep 1 [cited 2025 Jan 3];9(1):1723260. Available from: https://onlinelibrary.wiley.com/doi/full/10.1080/20013078.2020.1723260

89. Kim S, Lee SK, Kim H, Kim TM. Exosomes Secreted from Induced Pluripotent Stem Cell-Derived Mesenchymal Stem Cells Accelerate Skin Cell Proliferation. International Journal of Molecular Sciences 2018, Vol 19, Page 3119 [Internet]. 2018 Oct 11 [cited 2025 Jan 3];19(10):3119. Available from: https://www.mdpi.com/1422-0067/19/10/3119/htm

90. Hu GW, Li Q, Niu X, Hu B, Liu J, Zhou SM, et al. Exosomes secreted by human-induced pluripotent stem cell-derived mesenchymal stem cells attenuate limb ischemia by promoting angiogenesis in mice. Stem Cell Res Ther [Internet]. 2015 Apr 10 [cited 2025 Jan 3];6(1):1–15. Available from: https://stemcellres.biomedcentral.com/articles/10.1186/scrt546

91. Xia Y, Ling X, Hu G, Zhu Q, Zhang J, Li Q, et al. Small extracellular vesicles secreted by human iPSC-derived MSC enhance angiogenesis through inhibiting STAT3-dependent autophagy in ischemic stroke. Stem Cell Res Ther [Internet]. 2020 Jul 22 [cited 2025 Jan 3];11(1):1–17. Available from: https://stemcellres.biomedcentral.com/articles/10.1186/s13287-020-01834-0

92. Tang Q, Lu B, He J, Chen X, Fu Q, Han H, et al. Exosomes-loaded thermosensitive hydrogels for corneal epithelium and stroma regeneration. Biomaterials. 2022 Jan 1;280:121320.

93. Liang Q, Monetti C, Shutova M V., Neely EJ, Hacibekiroglu S, Yang H, et al. Linking a cell-division gene and a suicide gene to define and improve cell therapy safety. Nature. 2018 Nov 29;563(7733):701–4.

94. Bloor AJC, Patel A, Griffin JE, Gilleece MH, Radia R, Yeung DT, et al. Production, safety and efficacy of iPSC-derived mesenchymal stromal cells in acute steroid-resistant graft versus host disease: a phase I, multicenter, open-label, dose-escalation study. Nat Med. 2020 Nov 1;26(11):1720–5.

95. Elgaz S, Kuçi Z, Kuçi S, Bönig H, Bader P. Clinical Use of Mesenchymal Stromal Cells in the Treatment of Acute Graft-versus-Host Disease. Transfusion Medicine and Hemotherapy [Internet]. 2019 Feb 1 [cited 2025 Mar 14];46(1):27. Available from: https://pmc.ncbi.nlm.nih.gov/articles/PMC6558336/

96. Siegel G, Kluba T, Hermanutz-Klein U, Bieback K, Northoff H, Schäfer R. Phenotype, donor age and gender affect function of human bone marrow-derived mesenchymal stromal cells. BMC Med [Internet]. 2013 Jun 11 [cited 2025 Mar 14];11(1):1–20. Available from: https://bmcmedicine.biomedcentral.com/articles/10.1186/1741-7015-11-146

97. Kirkeby A, Main H, Carpenter M. Pluripotent stem-cell-derived therapies in clinical trial: A 2025 update. Vol. 32, Cell Stem Cell. Cell Press; 2025. p. 10–37.

98. Zhu Y, Xu L, Collins JJP, Vadivel A, Cyr-Depauw C, Zhong S, et al. Human Umbilical Cord Mesenchymal Stromal Cells Improve Survival and Bacterial Clearance in Neonatal

Sepsis in Rats. Stem Cells Dev [Internet]. 2017 Jul 15 [cited 2023 Apr 13];26(14):1054–64. Available from: https://pubmed.ncbi.nlm.nih.gov/28401804/

99. Dominici M, Le Blanc K, Mueller I, Slaper-Cortenbach I, Marini FC, Krause DS, et al. Minimal criteria for defining multipotent mesenchymal stromal cells. The International Society for Cellular Therapy position statement. Cytotherapy [Internet]. 2006 Aug [cited 2024 Dec 26];8(4):315–7. Available from: https://pubmed.ncbi.nlm.nih.gov/16923606/

100. Van Haaften T, Byrne R, Bonnet S, Rochefort GY, Akabutu J, Bouchentouf M, et al. Airway delivery of mesenchymal stem cells prevents arrested alveolar growth in neonatal lung injury in rats. Am J Respir Crit Care Med [Internet]. 2009 Dec 1 [cited 2025 Jan 7];180(11):1131–42. Available from: https://pubmed.ncbi.nlm.nih.gov/19713449/

101. Cyr-Depauw C, Cook DP, Mižik I, Lesage F, Vadivel A, Renesme L, et al. Single-Cell RNA Sequencing Reveals Repair Features of Human Umbilical Cord Mesenchymal Stromal Cells. Am J Respir Crit Care Med. 2024 Sep 15;

102. Siegel G, Schäfer R, Dazzi F. The immunosuppressive properties of mesenchymal stem cells. Transplantation [Internet]. 2009 [cited 2025 Apr 2];87(9 Suppl). Available from: https://pubmed.ncbi.nlm.nih.gov/19424005/

103. Fanaroff AA, Stoll BJ, Wright LL, Carlo WA, Ehrenkranz RA, Stark AR, et al. Trends in neonatal morbidity and mortality for very low birthweight infants. Am J Obstet Gynecol. 2007;196(2):147.e1-147.e8.

104. Siffel C, Kistler KD, Lewis JFM, Sarda SP. Global incidence of bronchopulmonary dysplasia among extremely preterm infants: a systematic literature review. Journal of Maternal-Fetal and Neonatal Medicine. 2021;34(11):1721–31.

105. Sangsari R, Saeedi M, Maddah M, Mirnia K, Goldsmith JP. Weaning and extubation from neonatal mechanical ventilation: an evidenced-based review. BMC Pulm Med [Internet]. 2022 Dec 1 [cited 2023 Apr 23];22(1):1–12. Available from: https://bmcpulmmed.biomedcentral.com/articles/10.1186/s12890-022-02223-4

106. Perrone S, Bracciali C, Di Virgilio N, Buonocore G. Oxygen Use in Neonatal Care: A Two-edged Sword. Front Pediatr. 2017 Jan 9;4.

107. Behrman RE, Butler AStith, Institute of Medicine (U.S.). Committee on Understanding Premature Birth and Assuring Healthy Outcomes. Preterm birth : causes, consequences, and prevention. Vol. 10. National Academies Press; 2007. 313–345 p.

108. Wong PM, Lees AN, Louw J, Lee FY, French N, Gain K, et al. Emphysema in young adult survivors of moderate-to-severe bronchopulmonary dysplasia. European Respiratory Journal. 2008 Aug;32(2):321–8.

109. Mourani PM, Dunbar Ivy D, Rosenberg AA, Fagan TE, Abman SH. Left Ventricular Diastolic Dysfunction in Bronchopulmonary Dysplasia. J Pediatr. 2008;152(2):291–3.

110. Goss KN, Beshish AG, Barton GP, Haraldsdottir K, Levin TS, Tetri LH, et al. Early pulmonary vascular disease in young adults born preterm. Am J Respir Crit Care Med. 2018 Dec 15;198(12):1549–58.

111. Northway W, Rosan R, Porter D. Pulmonary Disease Following Respirator Therapy of Hyaline-membrane Disease. N Engl J Med. 1967;276(7):357–68.

112. Summary Basis of Decision - Prochymal - Health Canada [Internet]. [cited 2025 Apr 25]. Available from: https://hpr-rps.hres.ca/reg-content/summary-basis-decision-detailOne.php?linkID=SBD00118

113. Cyr-Depauw et al. Defining the next-generation umbilical cord-derived cell therapy for treatment of bronchopulmonary dysplasia. Unpublished.

114. Wang Q, Li J, Wang S, Deng Q, Wang K, Dai X, et al. Single-cell transcriptome profiling reveals molecular heterogeneity in human umbilical cord tissue and culture-expanded mesenchymal stem cells. FEBS J [Internet]. 2021 Sep 1 [cited 2025 Apr 23];288(18):5311–30. Available from: https://pubmed.ncbi.nlm.nih.gov/33763993/

115. Sun C, Wang L, Wang H, Huang T, Yao W, Li J, et al. Single-cell RNA-seq highlights heterogeneity in human primary Wharton's jelly mesenchymal stem/stromal cells cultured in vitro. Stem Cell Res Ther [Internet]. 2020 Apr 6 [cited 2025 Apr 23];11(1):1–16. Available from: https://stemcellres.biomedcentral.com/articles/10.1186/s13287-020-01660-4

116. Jia Z, Wang S, Liu Q. Identification of differentially expressed genes by single-cell transcriptional profiling of umbilical cord and synovial fluid mesenchymal stem cells. J Cell Mol Med [Internet]. 2020 Jan 1 [cited 2025 Apr 23];24(2):1945–57. Available from: https://pubmed.ncbi.nlm.nih.gov/31845522/

117. Huang Y, Li Q, Zhang K, Hu M, Wang Y, Du L, et al. Single cell transcriptomic analysis of human mesenchymal stem cells reveals limited heterogeneity. Cell Death & Disease 2019 10:5 [Internet]. 2019 May 8 [cited 2025 Apr 23];10(5):1–12. Available from: https://www.nature.com/articles/s41419-019-1583-4

118. Barrett AN, Fong CY, Subramanian A, Liu W, Feng Y, Choolani M, et al. Human Wharton's Jelly Mesenchymal Stem Cells Show Unique Gene Expression Compared with Bone Marrow Mesenchymal Stem Cells Using Single-Cell RNA-Sequencing. Stem Cells Dev [Internet]. 2019 Feb 1 [cited 2025 Apr 23];28(3):196–211. Available from: https://pubmed.ncbi.nlm.nih.gov/30484393/

119. Zhang C, Han X, Liu J, Chen L, Lei Y, Chen K, et al. Single-cell Transcriptomic Analysis Reveals the Cellular Heterogeneity of Mesenchymal Stem Cells. Genomics Proteomics Bioinformatics. 2022 Feb 1;20(1):70–86.

120. Cai S, Fan C, Xie L, Zhong H, Li A, Lv S, et al. Single-cell RNA sequencing reveals the potential mechanism of heterogeneity of immunomodulatory properties of foreskin and

umbilical cord mesenchymal stromal cells. Cell Biosci [Internet]. 2022 Dec 1 [cited 2025 Apr 23];12(1). Available from: https://pubmed.ncbi.nlm.nih.gov/35869528/

121. Wang Z, Chai C, Wang R, Feng Y, Huang L, Zhang Y, et al. Single-cell transcriptome atlas of human mesenchymal stem cells exploring cellular heterogeneity. Clin Transl Med [Internet]. 2021 Dec [cited 2025 Apr 23];11(12). Available from: https://pubmed.ncbi.nlm.nih.gov/34965030/

122. Musiał-Wysocka A, Kot M, Majka M. The Pros and Cons of Mesenchymal Stem Cell-Based Therapies. Cell Transplant [Internet]. 2019 Jul 1 [cited 2025 May 3];28(7):801. Available from: https://pmc.ncbi.nlm.nih.gov/articles/PMC6719501/

123. Bonab MM, Alimoghaddam K, Talebian F, Ghaffari SH, Ghavamzadeh A, Nikbin B. Aging of mesenchymal stem cell in vitro. BMC Cell Biol [Internet]. 2006 Mar 10 [cited 2025 May 3];7. Available from: https://pubmed.ncbi.nlm.nih.gov/16529651/

124. Gobin J, Muradia G, Mehic J, Westwood C, Couvrette L, Stalker A, et al. Hollow-fiber bioreactor production of extracellular vesicles from human bone marrow mesenchymal stromal cells yields nanovesicles that mirrors the immuno-modulatory antigenic signature of the producer cell. Stem Cell Res Ther. 2021 Dec 1;12(1).

125. Lee HR, Kim S, Shin S, Jeong SY, Lee DW, Lim SU, et al. iPSC-Derived MSCs Are a Distinct Entity of MSCs with Higher Therapeutic Potential than Their Donor-Matched Parental MSCs. Int J Mol Sci [Internet]. 2023 Jan 1 [cited 2024 Apr 1];24(1). Available from: /pmc/articles/PMC9821152/

126. Rajasingh S, Sigamani V, Selvam V, Gurusamy N, Kirankumar S, Vasanthan J, et al. Comparative analysis of human induced pluripotent stem cell-derived mesenchymal stem cells and umbilical cord mesenchymal stem cells. J Cell Mol Med [Internet]. 2021 Sep 1 [cited 2025 Apr 23];25(18):8904–19. Available from: https://onlinelibrary.wiley.com/doi/full/10.1111/jcmm.16851

127. Kang R, Zhou Y, Tan S, Zhou G, Aagaard L, Xie L, et al. Mesenchymal stem cells derived from human induced pluripotent stem cells retain adequate osteogenicity and chondrogenicity but less adipogenicity. Stem Cell Res Ther [Internet]. 2015 Aug 18 [cited 2025 Apr 23];6(1):144. Available from: https://pmc.ncbi.nlm.nih.gov/articles/PMC4539932/

128. Lee HR, Kim S, Shin S, Jeong SY, Lee DW, Lim SU, et al. iPSC-Derived MSCs Are a Distinct Entity of MSCs with Higher Therapeutic Potential than Their Donor-Matched Parental MSCs. Int J Mol Sci [Internet]. 2023 Jan 1 [cited 2025 Apr 23];24(1):881. Available from: https://pmc.ncbi.nlm.nih.gov/articles/PMC9821152/

129. Renesme L, Cobey KD, Lalu MM, Bubela T, Chinnadurai R, De Vos J, et al. Clearing up the mesenchymal 'stem-cell' mess: Delphi-driven consensus definition and clinical reporting guidelines.

130. Cyr-Depauw C, Hurskainen M, Vadivel A, Mižíková I, Lesage F, Thébaud B. Characterization of the innate immune response in a novel murine model mimicking bronchopulmonary dysplasia. Pediatr Res [Internet]. 2021 Mar 1 [cited 2025 Jan 7];89(4):803–13. Available from: https://pubmed.ncbi.nlm.nih.gov/32434214/